NEXT GENERATION VEHICLE – ENGINEERING GUIDELINES FOR STAINLESS STEEL IN AUTOMOTIVE APPLICATIONS

S. Schuberth[1], E. Schedin[2], T. Fröhlich[3], E. Ratte[1]

[1]ThyssenKrupp Nirosta GmbH, Germany, [2]Outokumpu Stainless AB, Sweden, [3]ArcelorMittal Stainless Europe, France

Abstract

The objectives of the NGV (Next Generation Vehicle) Project were to demonstrate that stainless steel can be used to reduce weight and costs, and to improve safety and sustainability in structural automotive systems. The deliverables include enabling technologies, virtual technology for design and development, processing and testing. The compilation of the results as well as aspects such as new design criteria for the application of stainless steels in automotive components were arranged in an Engineering Guideline for car manufacturers and their suppliers. The program was approved by constructing several newly designed B-pillars where the deliverables were successfully applied. After performing some regular crash tests the cost efficiency was estimated by the NGV cost model. The NGV Project deliverables and data base establish a sound basis for the use of stainless steels in automotive series production.

Introduction

The automotive industry of today is characterized by faster cycles in materials invention, development and application, coupled with the ability to tailor materials for specific end-users requirements i.e. multi material solutions. It is therefore essential for materials development to be closely integrated with the final product and process concurrent engineering practice. This means being aware of

- the market and customers,
- industrial and environmental trends and forces,
- recycling,
- cost efficiency,
- and technology development.

The aim of the project is to point out to the automotive industry that stainless steel can be used to reduce weight and cost in the manufacture of motor vehicles and to improve safety and sustainability in automotive body structures. The competiveness of stainless steels should be approved in the same process steps which a standard automotive development follows: the virtual development supported by FE-simulations, the analysis of forming, tooling, joining and determination of surface and corrosion properties. These different areas mark the structure of the NGV Project. The material choice for the project and the main results of the different research areas are explained in the following.
Because of the complexity of the topic and the large experimental effort the project was organised by the three stainless steel producers ThyssenKrupp Nirosta GmbH , ArcelorMittal Stainless and Outokumpu Oyj. The European car manufacturers were represented by AUDI AG,

BMW AG, Daimler AG, Saab Automobile AB, Volvo Cars and the Centro Ricerche Fiat. For the different working groups experts were integrated to ensure that the experiments conducted are according to the current state of the art.

Material

Traditionally, stainless steels are classified mainly by their microstructure. The major basic groups are martensitic, ferritic, austenitic and duplex (austenitic & ferritic) materials. The area of use for stainless steels is very vast and comprises mainly applications taking advantage of properties such as resistance against corrosion and/or very high or low temperatures as well as hygienic surfaces and aesthetic appearance. Increasingly, stainless steels are being used also for their mechanical properties such as the combination of very high strength and excellent formability together with high energy absorption capability in finished components. The stainless steels used in the NGV Project are all but one austenitic and that one is duplex, Table 1. The chemical composition of the different grades is given in Table 2.

Table 1. Material selection for the NGV Project

EN	Type	Finishing	Supplier
1.4376	Austenitic	2B[1]	ThyssenKrupp Nirosta (TKN) ArcelorMittal Stainless Europe (AMSE) Outokumpu (OS)
1.4318 1.4318 C1000	Austenitic	2B[1] Temper C1000[2]	
1.4310 1.4310 C1000	Austenitic	2B[1] Temper C1000[1]	
1.4162	Duplex	2E[3]	

[1] Cold rolled, annealed to retrieve material properties after cold rolling, pickled and skin passed
[2] Reduced by cold rolling and achieved desired mechanical properties maintained, C1000 stating the tensile strength
[3] Cold rolled, heat treated, mechanically descaled and pickled

Table 2. Chemical composition of materials investigated

Grade	C	N	Cr	Ni	Mo	Mn
1.4376	0.03	0.19	17.6	4.2	0.15	6.5
1.4318	0.025	0.11	17.5	6.6	0.20	<1.3
1.4310	0.10	0.03	17.0	7.0	<0.6	<2.0
1.4162	0.03	0.22	21.5	1.5	0.30	5.0

The austenitic materials referred to in these Guide Lines have mostly a more or less pronounced unique feature and that is deformation- or strain-induced hardening through a forming of martensite in the material. Thus facilitating cold rolling to very high strength levels or creating strength during forming operations.

Mechanical properties

Tensile tests on stainless steels are done according to EN 10002 standard, i.e. specimen geometry and preparation, test conditions (position relatively to the rolling direction, temperature indicated, etc). Tests are typically performed at room temperature (296 K), on as-received material in the three directions (0°, 90° and 45°). The mechanical properties and r-values are summarized in Table 3. The n-value is generally determined according to the standard above mentioned; computed between 18-40% for annealed grades and between 5-17% for temper rolled C1000 grades. Even if n-values are available, they are not very meaningful when

considering austenitic stainless steels prone to deformation martensite formation since they do not describe the complete curve. Figure 1 shows such an example in the case of 1.4318 where the Hollomon model cannot fit the tensile curve because of two slopes due to the TRIP effect.

Table 3. Mechanical Properties (non-isothermal test conditions)

Value (unit)	1.4376	1.4318	1.4318 C1000	1.4310	1.4310 C1000	1.4162
$Rp_{0.2}$ (MPa)	410	420	800	300	950	600
Rm (MPa)	740	765	1050	800	1050	840
A80 (%)	40	35	18	45	25	30
R_0	0,83	0,89	0,61	0,97	0,97	0.68
R_{45}	0,96	0,98	0,62	0,97	0,97	0.65
R_{90}	0,88	0,92	0,80	0,96	0,96	0.82

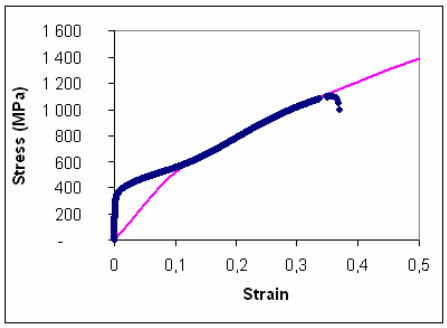

Figure 1. Comparison between the Hollomon model and the tensile curve for 1.4318

The materials here described are however not only prone to hardening through phase transformation but the rate of transformation is also dependent on strain rate as well as temperature. Consequently data from different temperature histories are of importance for forming simulation and for softwares to be able to handle those parameters. Additional to the standard tensile testing non-isothermal tests and isothermal tensile tests were conducted to determine the parameters necessary to fit the models describing the martensite formation. Additional to the quasistatic tensile tests, dynamic material properties were investigated according to the PUD-S (Prüf- und Dokumentationsrichtlinie now SEP 1240 [3]). The dynamic material properties are measured in high speed tension tests at 1, 10, 100 and 250 s^{-1}.
For a complete material description in FE-simulation the knowledge about a suitable failure criteria is necessary. The most common experimental techniqueis the Nakajima method. Test specimens and conditions follow generally the PUD-S. Some differences or adaptations particular for stainless steels can occur in specimen geometry (not parallel length for sample) stamp diameters (100mm is standard for thick and temper 50 or 75 mm can be used) or in multilayer lubrification system.
The material properties are completed by fatigue tests. Wöhler curves (high cycle fatigue data), Manson-Coffin curves (low cycle fatigue) and cyclic hardening data are available on some NGV grades.

Simulation

Development of Input-data

The occurring TRIP-effect has a great impact of the forming behaviour and the resulting strength. Consequently the material models which are implemented into the FE-code have to consider the martensite formation and the resulting hardening. Additionally, it needs to provide a forming history containing information about the resulting strength distribution and thereby facilitating a correct base for crash simulation.
Two different material models, both considering the TRIP-effect and its temperature sensitivity, have been used for the project. The first model is the Hänsel-Model [1]. For the implementation two minor additions were made which avoid on the one hand that the hardening modulus will approach infinity as the plastic strain reaches zero and on the other hand the initially used yield surface according to von Mises was replaced by that of Barlat and Lian. The second model used

is the Guimares model [2]. One major difference between the models is the different number of parameters which is 13 for the Hänsel model and 4 for the Guimares model. The resulting material behaviour was implemented with a simple mix-law.
The failure prediction in FE-simulations is usually done by comparing the strain distribution in critical areas with experimental FLC. Following the discussion above the best would be to use a range of FLC, determined at different temperatures. Until such data are available or a better solution exists, i.e. the numerical determination of forming limits, it is recommended to use the FLC at room temperature as the best approximation.
After the validation of the above mentioned input-data (Figure 2 shows a deep drawn component with calculated martensite fraction), a B-pillar reinforcement was simulated using the modified Hänsel model. The crash simulation was validated with two different components: a rectangular tube was crashed in compression comparable to those crash boxes which are placed behind the bumper of a car. The second validation was done with a 3-point bending geometry (Figure 3) which was chosen because it has the same crash mode as a B-pillar which is bending. Both tests were simulated and compared to the experimental results. The prediction of forces could be improved by using the modified Hänsel model in forming and crash simulation [1].

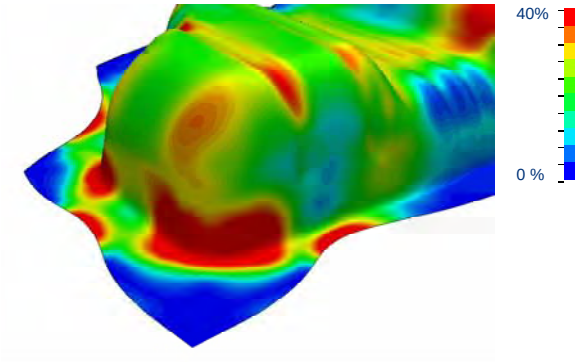

Figure 2. Simulated martensite volume

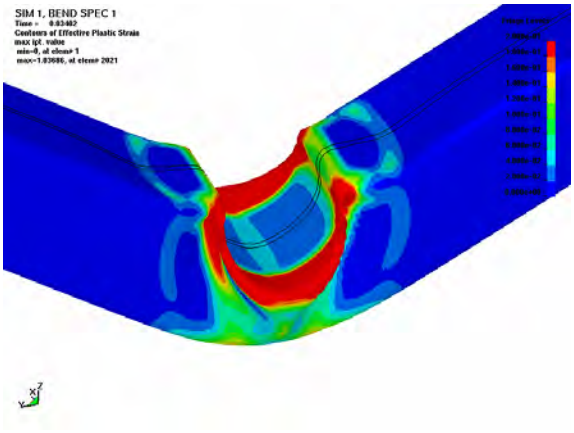

Figure 3. Simulated 3-point bending sample

Tooling

Stainless steels can in general be formed and worked by conventional processes. It is however important to remember the work hardening effects during processing which result in similar recommendations as those for high strength carbon or multiphase steels. These are of course the consideration of the higher punch- and blankholder-forces, necessary modifications of the draw bead restraining force, the use of more efficient tool material and coatings especially in critical areas as well as an optimized lubrication.
In the experiments for piercing and trimming the stainless steels 1.4376 and 1.4318 C1000 were compared. The used tool material was X70CrMoV5-2 (“Caldie”). Three different coatings, TiAlN, AlCrN, TiC were compared. Coatings were approved when at least 100.000 holes can be pierced without any burr height exceeding 60 µm and without any fatigue cracks or chipping tendencies present in the punches. For the TiC and TiAlN coatings the burr height when piercing 1.4376 is 25 µm in average. The punch force amounts to 30 N, the punch work increased during the test from around 18 J up to 20 J. Only in spalling differences between the two coatings could be observed. TiAlN did not show any signs of spalling whereas TiC showed spalling at the punch edges. Figure 4 shows the piercings at the beginning and after 100.000 strokes. Additionally, the punches after 100.000 strokes are depicted. These results show that it exists combinations of tool material/tool coating/lubricant that enable to pierce and trim stainless TRIP steels grades (fulfilling the demands from the automotive industry).

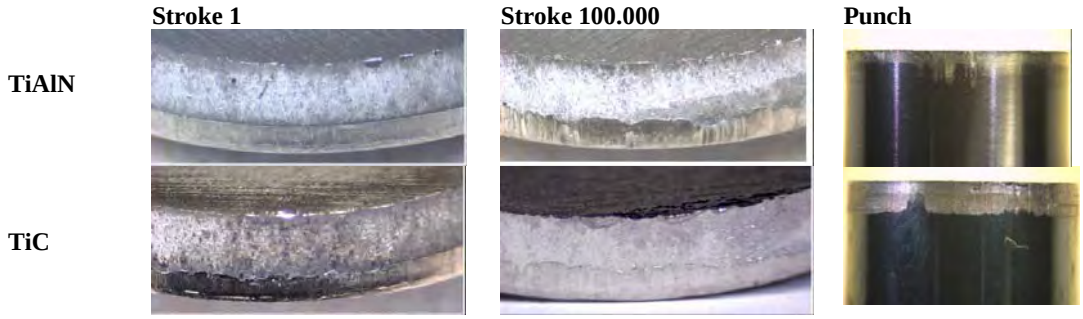

Figure 4. Comparison of piercings at the beginning and after 100.000 strokes

Joining

Stainless steels can be joined to each other as well as other materials with most common joining methods. To some extent deviations in parameters compared to what is common for mild carbon steels are inevitable. Main issue about joining stainless steels are the different physical properties compared to carbon steels that lead to different parameters compared to other steels or alloys (Table 4). Beside stainless-stainless combinations, emphasis was laid on the exploration of mixed combinations.

Table 4. Physical properties of stainless steels and other alloys

Grade	Thermal conductivity at 20°C W* m -1 * K -1	Spec. electrical resistance at 20°C Ω * mm² /m	Thermal expansion in 10-6 K-1between 20°C and 100°C
DC03 (ferritic deep drawing C-steel) DX54D (ferritic deep drawing C-steel)	50	0,22	12,0
1.4310 1.4376	15	0,73	16,0
Ecodal 6181 (AlMgSi 0.8 alloy)	≥ 190	0,033	23,4

Altogether five different processes were covered experimentally. These were resistance spot welding for stainless-stainless and mixed combinations in two and three sheet joining, resistance spot welding with an additional adhesive bonding, laser welding, MAG-welding, and adhesive bonding. After joining, the different combinations were tested in cyclic tests, the bonded samples in shear and peel-tests. Welded joints were additionally tested in corrosive environments which will be discussed in the next chapter. Due to the large experimental part, only some exemplary results can be depicted in this manuscript.

Figure 5 shows the results for fatigue testing of spot welded and spot welded samples with additional bonding. The adhesive used is Betamate 1496, which is a one component, epoxy based adhesive manufactured by Dow Automotive. The additional bonding leads to a large rise in the measured loads amplitudes, both, for stainless-stainless joints and for the mixed joint of 1.4376-DC03+ZE. The same tendency could be observed for the other combinations investigated.

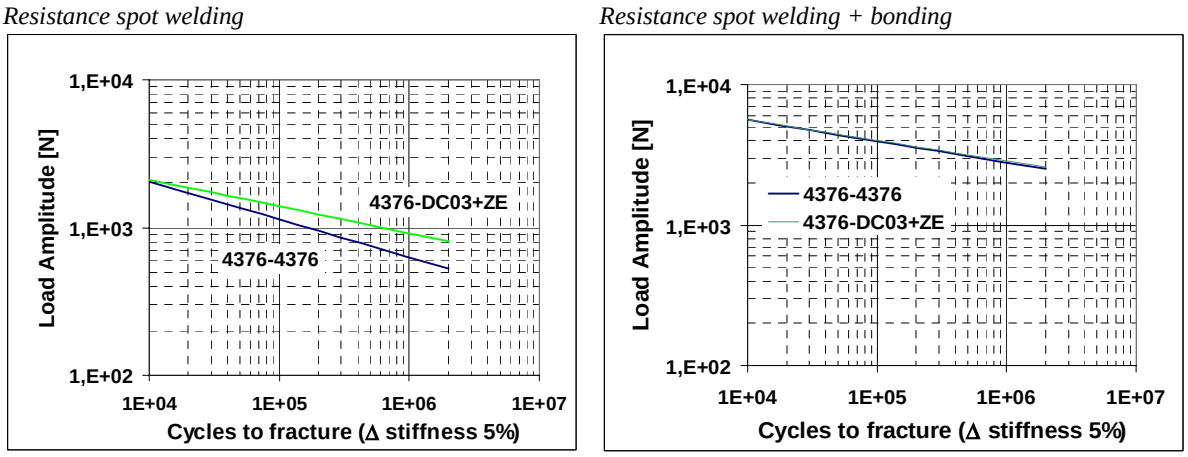

Figure 5. Comparison of fatigue tests of spot welded and spot welded + bonded samples Graph for 50% -Break down probaility, R=0,1 / f=90 Hz / T=25°C

Tailor welded blanking is an interesting method for optimizing components in regards of function as well as weight. Stainless steel can readily be used for that purpose in combination with other stainless steels or even with carbon steels which works with very good results as can be seen in Figure 6. Important factors to consider in laser welding are the laser power, the welding speed, the intensity of allocation, the focus diameter, the edge quality and positioning and the gas distribution.

Figure 6. Microcraphs of stainless-stainless and mixed laser weld, tailor welded blank

The most significant overall statements of the joining investigations were that stainless steels are weldable to each other and in mixed material joints. When employing resistance spot welding a higher electrode force might be necessary. MAG welding is suitable as well, but as for coated carbon steels, joints of stainless and coated carbon steels may show porosities. In laser-welding attention should be paid to the clampings and evaporation of zinc in dissimilar joints. The bonded joints show good values in shear and peel test.

Surface and Corrosion

Due to the passive layer stainless steels are resistant to humid atmosphere and to pure water, keep a bright shiny and stainless surface, and do not show rust as unalloyed steels and iron do. Generally, corrosion does only occur in very aggressive media (strong acids or hot strong alkalis) where the surface oxide film is not stable anymore. More relevant for daily life applications are forms of localized corrosion such as pitting and crevice corrosion. Stress corrosion cracking which can develop under very specific conditions included the effect of media bearing chloride ions. Consequently, the surface and corrosion part will primarily deal with forms of localized corrosion which may become relevant for automotive applications of stainless steels. In addition,

strategies for avoiding galvanic corrosion when pairing stainless steels with less noble materials are discussed.
Especially after resistance spot welding the joint may be affected by localized corrosion and stress corrosion cracking. To avoid corrosion of the joints the seam can be protected by wax, by coatings which provide a cathodic protection, or in case of the spot welds with adhesive bonding by the adhesive, Figure 7.

RSW RSW+Bonding RSW+Bonding

Figure 7. RSW not protected with rust formation, and RSW which are protected by the bonding after salt spray test

Implementation of knowledge gained in B-pillar concepts

One major aim of the project was to transfer the knowledge gained as fast as possible to a new product development. Therefore each car manufacturer developed a B-pillar design as a mixed material concept. The concepts differed in terms of material choice, forming procedure and joining techniques, Table 5.

All of the concepts investigated lead to a decrease of weight compared to the reference concept which is fully made of carbon and multiphase steel. To check the cost efficiency of the newly developed concepts a calculation of costs was done. Based on the parameters of the ULSAB-study a calculation tool was developed which allows a closer view on the costs of the different processes, materials and joining techniques. Assuming that the maximum scrap volume does not exceed 40% of the initial blank size, concept C and E without otimization come already close to the reference concept.

Table 5. B-Pillar concepts of the NGV project not optimized

B-Pillar	**Reference**	**C**	**E**
Material	Rephos DP600	Rephos 1.4310-C 1000 + DP 600	Rephos 1.4310-C 1000 + DP600
Process	Tailor weld	Tailor weld	Rollform
Δ Wght	**-**	- 3.51 kg	- 4.81 kg
Δ Cost/ Δ Wght		4,40 €	0,40 €

To compile the results from the different work packages, two B-pillars (concept Hydroforming and Concept Stamping with tailor welded blanks) were on the one hand virtually designed which includes the forming simulation of e.g. the hydroformed parts, the mapping of results for the crash simulation and the crash simulation itself (Figure 8). On the other hand they were produced and crash-tested. A comparison of acceleration as function of time showed a good matching of the calculated level with the experimental results. The analysis of the maximum displacement reveiled, that the simulation underestimates the intrusion which might be due to a overestimation of calculated strength. Nevertheless, the results show that a continuous simulation is possible and already comes to reasonable results. In the future the underlying models should be further adapted to optimise the simulated results.

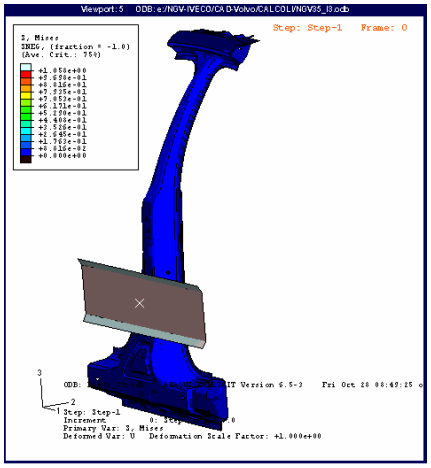

Figure 8. Model for crash-simulation

Figure 9. B-pillar for experimental crash-test

Conclusions

- Stainless steels show very good combinations of strength and ductility which is of special interest in automotive applications. The use of this materials presuppose the safe and correct use in all stages automotive development and production.
- In virtual development, the description of the material behaviour could be improved by the implementation of temperature sensitive models which allow the prediction of martensite and thus a more accurate strength determination in the virtual modelling.
- In tooling and forming stainless steels show the same restrictions as high-strength carbon steels do. Coatings such as TiAlN withstand the high forces and allow an accurate forming.
- Joining of stainless steels in uni-material and mixed joints is possible. In some cases deviations in parameters compared to what is common for mild carbon steels are inevitable but in general not greater than for different grades of carbon steel.
- To avoid corrosion of the joints the seam can be protected by wax, by coatings which provide a cathodic protection, or in case of the spot welds with adhesive bonding by the adhesive to ensure a continuity of the corrosion resistance.
- The implementation of the results into the design of several B-pillar concepts shows on the one hand the potentials for a further weight reduction and on the other hand the cost efficiency of some concepts. Designing with stainless steel need not necessarily to be adversarial compared to mild and multiphase steels especially in terms of weight savings and by the same time reasonable costs.

References

[1] A.H.C. Hänsel, P. Hora, and J. Reissner, “Model for the kinetics of strain-induced martensitic phase transformation at non-isothermal conditions for the simulation of sheet metal forming processes with metastable austenitic steels”, Simulation of Materials Processing: Theory, Methods, and Applications, Huétink and Baaijens (eds), Balkema, Rotterdam ,1998

[2] P.-O. Santacreu, J.C. Glez, N. Roulet, T. Fröhlich, Y. Grosbety, “Austenitic Stainless Steels For Automotive Structural Parts”, SAE papers 2006-01-1215

[3] Stahl-Eisen-Prüfblatt (SEP) 1240: “Prüf- und Dokumentationsrichtlinie für die experimentelle Ermittlung mechanischer Kennwerte von Feinblechen aus Stahl für die CAE-Berechnung”.

CORROSION RESISTANCE OF STAINLESS STEELS TO WET CONDENSATES IN AUTOMOTIVE EXHAUST SYSTEMS

P. Gümpel[1], C. Hoffmann[1], N. Arlt[2]

[1]University of Applied Sciences Konstanz, Germany, [2]ThyssenKrupp Nirosta GmbH, Germany

Abstract

The special corrosion conditions in the rear section of automotive exhaust systems make high demands on the stainless steels used for these components. Condensates bearing appreciable chloride ion concentrations and often low pH-values together with particles of electrochemical active soot can lead to pronounced pitting and crevice corrosion on the inner surfaces. Various steel grades are used, ferrites with different contents of chromium and molybdenum as well as austenitic types. For selection of an appropriate material enabling cost-effective constructions the corrosion resistance of different candidate grades has to be rated.

To gain more insight into the mechanism of corrosion occurring in exhaust systems and the effect of the different alloying elements investigations simulating these special corrosion conditions were carried out. They comprised the impact of acidic chloride bearing media and the influence of electrochemical active carbon as well as the effect of alternating wet-dry cycles. Electrochemical investigations dealt with initiation, growth and repassivation of pitting and crevice corrosion. The effect of geometrical effects on crevice corrosion was investigated. Electrochemical active carbon showed a pronounced effect on the corrosion behavior by raising the free corrosion potential. Beside the step of pitting and crevice corrosion initiation also growth and repassivation influenced materials performance. Thus the alloying elements chromium and molybdenum showed a beneficial effect by increasing resistance to initiation of localized corrosion whereas nickel improved corrosion behavior by retarding growth of corrosion sites. So the PRE-concept (pitting resistance equivalent) is not sufficient to rate the corrosion resistance of stainless steels to wet condensates in exhaust gas systems.

By giving a better understanding of the different alloying element effects on corrosion resistance the investigations provide valuable information for material development. In addition the study points out factors which are relevant for tests simulating the specific corrosion conditions in automotive exhaust systems.

Introduction

Automotive exhaust systems are complex constructions with different sections placing different demands on the materials.

Various stainless and heat-resistant steel grades are used to achieve an optimal combination of properties in each section.

From the standpoint of corrosion, exhaust lines may be divided into three parts:

- The front part (manifold pipes, catalytic converter), subjected mainly to high temperature oxidation.
- The centre section of the exhaust system (centre muffler, connecting pipes) subjected to both: high temperature oxidation with short periods of wet corrosion due to the condensates (internal parts) or road salt projection (external parts).

- The rear part (rear muffler), exposed to lower temperature and subjected mainly to wet corrosion by condensates (internal parts) or by road salt projection (external part). Inside the system, condensation of combustion gases produces sulphurous acid, sulphuric acid and low levels of hydrochloric acid, creating critical conditions with acidic pH-values. These condensates, combined with an accumulation of chloride ions and deposits of electrochemically active soot particles, can result in substantial wet corrosive impact on the inner surfaces of the components.

To compare the suitability of various stainless steels concerning their application in the wet sections of automotive exhaust systems, technological tests are carried out which take into account the specific features of this corrosion impact. The following factors must be considered:

- The wet/dry alternation
- The impact of a chloride ion-containing acidic medium
- The presence of electrochemically active carbon (occurring as soot particles in the systems)

The tests are carried out on ferrites, austenites and manganese–austenites.
The effect of the unburned carbon on the corrosion is examined with electrochemical methods.
The repassivation ability of corrosion pits of different stainless steel grades is examined in cyclic measurements.

Experimental

Technological Tests

Deep drawn specimens from strip of selected materials (Table 1) were used for the tests.

Table 1. The alloying composition of the specimens

Stainless steel grades	Alloying additions [wt %]			
	Cr	Ni	Mo	Mn
Cr-Steel 1.4512	11.54	-	-	-
Cr-Steel 1.4509	17.59	-	-	-
CrMo-Steel 1.4526	16.86	-	0.983	-
Cr NiMn-Steel 1.4376	18.93	3.33	-	7.7
CrNi-Steel 1.4301	17.88	9.08	-	-
CrNiMo-Steel 1.4404	16.36	11.88	1.84	-

The specimens were pickled and weighted before each test. They were filled with a corrosive medium and then exposed in a climate chamber at a defined temperature and humidity. A specimen underwent several cycles of being filled with corrosive medium and drying. After completing a pre-set number of cycles, the specimen were cleaned, its mass loss measured and the visual appearance of the corrosive attack assessed. The exposure conditions and the composition of the corrosive medium were varied to optimize the process.

Test with Electrolyte of pH 4

The specimens were filled with 10ml of the corrosive medium with a composition shown in Table 2. The specimens were placed in a climate chamber for 12 hours at 85°C and 50% relative humidity, and then for another 12 hours at 23°C and 50% relative humidity . During the first 12 hours an accelerated drying of a part of the electrolyte has taken place. On the surface where the electrolyte could evaporate, the crystallization of sodium chloride was observed. In the next

12 hours, due to the air humidity the crystallized salt would also provide a corrosive medium. After 24 hours the electrolyte was replenished. After 12 cycles, the specimens were cleaned, examined for corrosive attack and weighed. The test lasted 48 cycles.

Table 2. The composition of the electrolyte of pH 4

Electrolyte of pH 4	
Chemicals	**Amount**
Acetate buffer solution	1000ml
Sodium chloride	3.3g
Active carbon	1g

With both Diesel and Otto engine the condensates reach low acidic pH-values under certain conditions. In the test with electrolyte of pH 2.6, this corrosion factor, i.e. the acidic medium, simulated the most aggressive conditions in auto exhaust system. Further a reduction in duration of the technological tests was achieved; the test with electrolyte of pH 4 took comparably long, i.e. about two month.

Table 3. The Composition of the electrolyte of pH 2.6

Electrolyte of pH 2,6	
Chemicals	**Amount**
Citric acid – phosphate buffer solution	1000ml
Sodium chloride	3.3g
Active carbon	0.1g

The specimens were filled with 20ml of the corrosive medium with a composition shown in Table 3. As in this pH interval the buffering activity of the acetate buffer solution is no longer effective, citric phosphate buffer solution was alternatively chosen. The specimen with electrolyte were placed in a climate chamber for 12 hours at 85°C and 75% relative humidity, and then for another 12 hours at 23°C and 75% relative humidity. After 24 hours the electrolyte was replenished. Three specimens from each steel grade were placed in the climate chamber at the same time. After 3, 5 and 7 cycles respectively, one specimen from each steel grade was cleaned, examined for corrosive attack and weighed. The progressive investigation mode of the specimens revealed that already after few cycles, some specimens have broken through, which probably results from the very aggressive corrosive medium.

Electrochemical Measurements

Open-Circuit Potential

The influence of the unburnt carbon on corrosion effects was examined by measurement of the open-circuit potential from the different stainless steels grades, with and without active carbon, in electrolyte of pH 4 (Table 2), for about 24 hours. Thereby the electrolyte was saturated with oxygen. The active carbon was located on the concave surface of the specimen. The specimens were pickled before each test.

Cyclic Potentiodynamic Polarisation

The repassivation ability of different stainless steel grades was studied with the triangular voltage method. The applied potential on the specimen was linearly increased with a scan rate of 50mV/h. The start potential was 207mV against the standard hydrogen electrode and the current limit was 0.6mA. The applied potential was increased in the anodic direction until the measured current reach the current limit, after that the polarisation direction was reversed with the same

scan rate (50mV/h) back to the start potential. A 0.3% sodium chloride solution of pH 7-8 was used for electrolyte. The samples are fixed with crevice corrosion bodies in order to simulate the crevice conditions in the car exhaust system.

Results

Technological test with Electrolyte of pH 4

The nature of the corrosion attack is determined by various effects: both classic pitting and uniform attack are observed. The results of these tests are summarized in Figure 1. The mass loss and the differentiation among the grades increase with the number of cycles. The highest resistance is achieved by grade 1.4404, which confirms the positive influence of the alloying element molybdenum on the resistance to the onset of corrosion and the positive influence of the alloying element nickel on the repassivation during the idle periods. The grades 1.4526, 1.4301, 1.4376 and 1.4509 display no significant differences in mass loss. The grade 1.4512 with the lowest chromium content shows the highest mass loss. A relatively good agreement is observed between the mass loss rates and the alloy content of the materials. But based on the pitting attack mechanism the results of the mass loss measurements should always be treated with caution.

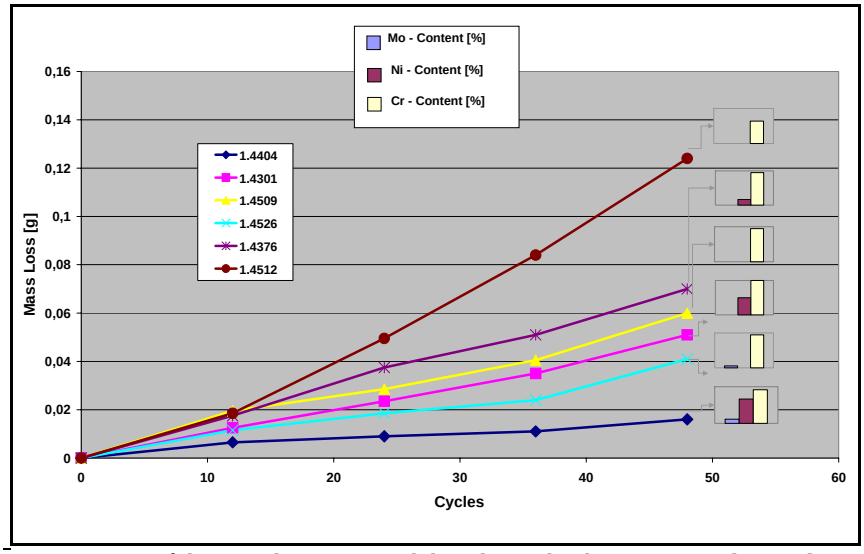

Figure 1. Run of the mass loss curve and the relationship between mass loss and Mo-, Ni-, Cr-contents, test with electrolyte of pH 4

Technological Test with Electrolyte of pH 2.6

The nature of the corrosion attack on the specimens of the grades 1.4404, 1.4526, 1.4509 and 1.4301 consist of classic pitting and uneven local attack. There is no uniform attack. With the new electrolyte, i.e. citric phosphate buffer solution, the corrosion mechanism is changing. The corrosive attack is more pronounced, so that some of the specimens are broken through after few cycles: steel grade 1.4526 after 4 cycles and 6 cycles, respectively, and steel grade 1.4301 after 3 cycles and 4 cycles, respectively. The mass loss after 3, 5 and 7 cycles in the climate chamber is shown in Figure 2, it also include the number of cycles until the steel grade 1.4301 and 1.4526 are breaking through.

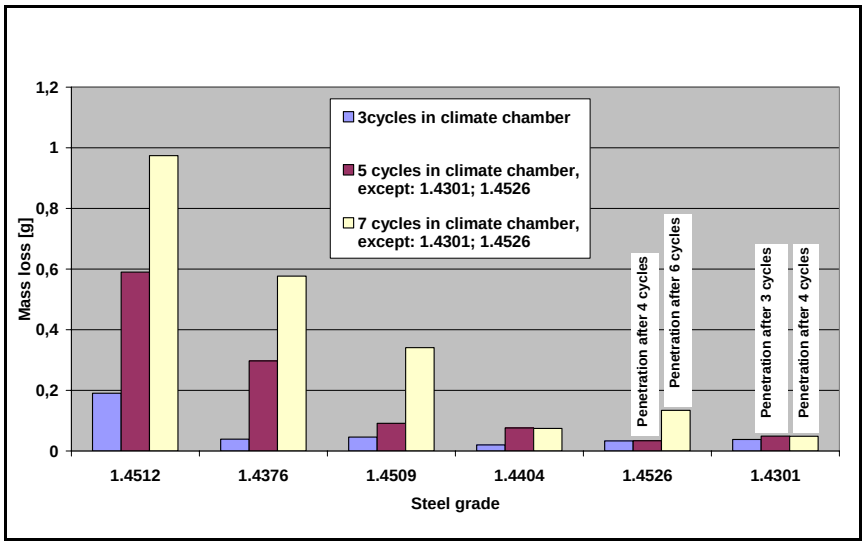

Figure 2: Mass loss after 3, 5 and 7 cycles respectively, test with electrolyte of pH 2.6

It can thus be demonstrated that there is no relationship between mass loss and the breaking through of the specimens. To compare the susceptibility of various stainless steels under aggressive pitting corrosion conditions, the mass loss measurements are less suitable.

Open-Circuit Potential Measurement

The run of the open-circuit potential curve for the different stainless steel grades shows a shift of the open circuit potential to higher values for the tests with active carbon in comparison to the tests without active carbon (for example Figure 3), which indicates an increasing susceptibility to pitting corrosion.

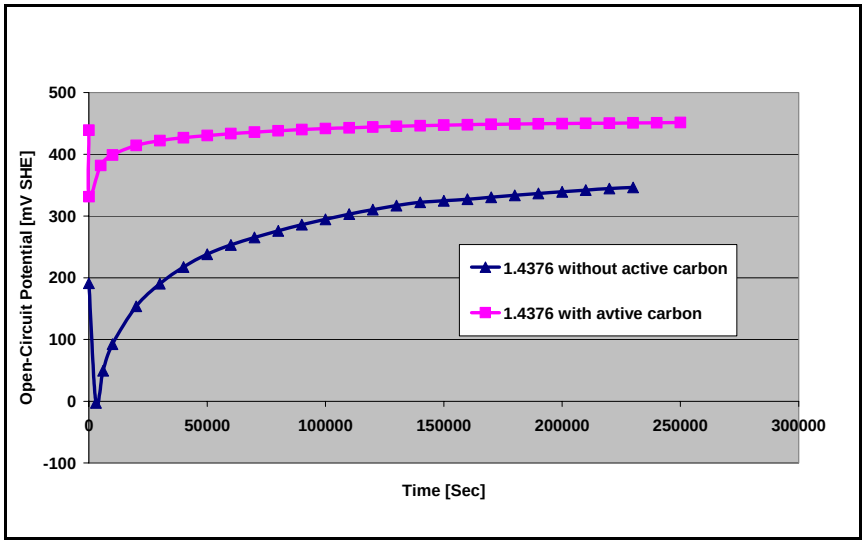

Figure 3. Run of the open-circuit potential curve, steel grade 1.4376 without and with active carbon

Cyclic Potentiodynamic Polarisation

From the run of the curves it can be notice that after initiation and growth, when the current density begins to decrease, i.e. repassivation, the descent of the current density for the austenites is more rapidly than for the ferrites (Figure 4 to 5) The existent pits are able to repassivate more quickly due to the favourable effect of the nickel content.

The repassivation ability of the different steel grades is compared on the basis of the potential interval during the current density descent.

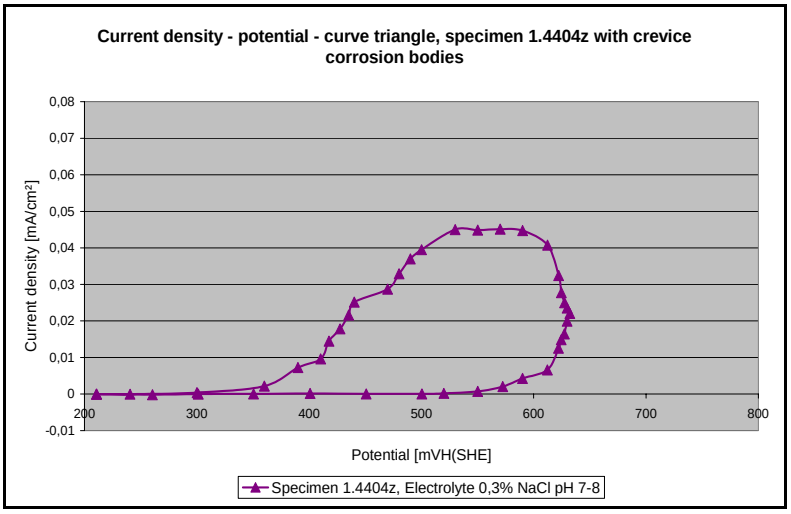

Figure 4. Cyclic potentiodynamic polarisation, steel grade 1.4404

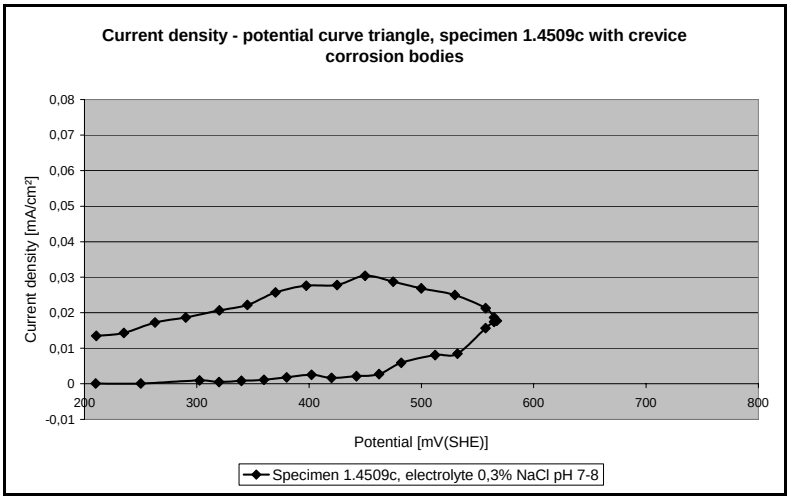

Figure 5. Cyclic potentiodynamic polarisation, steel grade 1.4509

Conclusions

For the corrosion conditions in the rear muffler the steel grade is 1.4512 overtaxed.
In the technological and electrochemical tests the steel grade 1.4404 exhibits a better resistance. The results of the tests confirm the beneficial effect of the alloying elements chromium and molybdenum by increasing the resistance against initiation of localized corrosion and the favourable effect of the alloying element nickel on the repassivation ability of the stainless steel.
The simulation tests with alternating wet/dry phases are most suitable to reflect the particular corrosion conditions in automotive exhaust systems. Their further development includes:

- Definition of an electrolyte with a proper buffer solution for the test conditions
- An appropriate method of valuation of the corrosion attack

References

[1] "Nichtrostende Stähle für Abgassysteme im automobil", Firmenschrift der Thyssen Krupp Nirosta

[2] P.Gümpel, "Rostfreie Stähle", 3. Auflage, Expert Verlag, 2001

[3] P.-J. Cunat, "Stainless Steel –Stainless Steel Properties for Structural Automotiv Applications", Paper present on: Metal Bulletin International Automotive Materials Conference, Cologne, 21st to 23st June 2000

[4] J. Kemppainen, "Stainless Steel – A New "Light Metal" for the Automotive Industry", Paper presented in Euro Inox Presentation Stainless Steel in Structural Automotive Industry Applications – Properties and Case Studies, Paris Motor Show Mondial de l'Automobil, 2nd October 2000

[5] J. Lagier, P. Rombeaux, J. Ragot, P. Vaugeois, "Ferritic Stainless Steels in Exhaust Systems", Innovation Stainless Steel, Florence, Italy, 11-14 October 1993

[6] P. Gümpel, D. Schiller, N. Arlt, D. Bouchholz, "Simulation des Korrosionsverhaltens von nichtrostenden Stählen in Pkw-Abgasanlage", Automobil Technische Zeitschrift, 4/2004

[7] H. Weltens, P. Garcia, H.-D. Walther, "Innen- und Außenkorrosion von Abgasanlagen für Pkw – Prüfverfahren, Labor- und Feldergebnisse", Vortrag, gehalten auf dem Dvm–Tag 1998

[8] Yoshiharu Inoue, Masao Kikuchi, "Present and Future Trends of Stainless Steel for Automotive Exhaust System", Nippon Steel Technical Report No. 88, July 2003

[9] E. Heitz, R. Henkhaus, A. Rahmel, "Korrosionskunde im Experiment", 2. Auflage, VCH Verlaggesellschaft mbH, 1990

ACE P439A: ACESITA'S GRADE FOR HIGH TEMPERATURE APPLICATION IN VEHICLE EXHAUST SYSTEM

R. A. Faria[1], P. O. Santacreu[2], H. J. B. Alves[1], T. R. Oliveira[1], R. P. Barbosa[1]

[1]ArcelorMittal Inox, Brasil, [2]ArcelorMittal, France

Abstract

ACE P439A (UNS 43932) has a high application versatility in automotive, sugar & alcohol mills and white goods industries, in function of its excellent properties such as: corrosion resistance, weldability and drawability. Concerning the automotive industry, ACE P439A has been mostly used in the "cold part" of vehicle exhaust systems. The present paper describes the evaluation of the high temperature properties of ACE P439A compared to the standard Ti mono stabilized grade (AISI 439) and the commonly used dual stabilized (AISI 441), in order to verify its application in the "hot part" of vehicle exhaust systems. ACE P439A has presented an intermediated behavior between the others two grades. This study has shown that it can be used at up to 850°C, while AISI 441 must be used for higher temperatures.

Introduction

Vehicle exhaust systems have evolved greatly in the last 20 years because of environmental laws and high lifetime guarantee. Ferritic stainless steels have become interesting because of its lower cost than austenitic ones and higher competitiveness than aluminized C steels and cast iron.[1,2,3]. Microstructure analysis has shown that creep resistance improvement of ferritic stainless steels is related to formation of Laves phase and the grain size has a little significant effect.[4,5,6] The mechanical properties of ferritic stainless steels depend strongly on the temperature and applied strain range.[7]

The aim of this paper is to evaluate the use of ACE P439A in the hot part of the exhaust system, where grade AISI441 is used. For this, a comparison with others grades and some mechanical tests and analysis were performed, in addition to industrial performance evaluation.

Materials

The studied ferritic stainless steels are stabilized (Ti, Nb or Ti+Nb with a nominal thickness of 1.50mm). Titanium and niobium free in solid solution (ΔTi and ΔNb) were determined by the equations shown in Table 1.[8,9]

Table 1. Chemical composition of stainless steels (% wt).

ASTM	Cr	C	N	Ti	S	Nb	ΔTi	ΔNb
ACE P439A	17,05	0,011	0,013	0,20	0,0015	0,19	0,14	0,14
AISI 439	16,26	0,026	0,011	0,47	0,0027	0,01	0,34	---
AISI 441	17,67	0,017	0,020	0,15	-----	0,50	0,06	0,41

$\Delta Ti = Ti - 3.42\ N - 4\ C$ Ti stabilized steels

$\Delta Nb = Nb - 7.74\ (C+N)$ Nb stabilized steels

$\Delta Ti = Ti - 3{,}42\ N - (0.30 \times 4C)$

$\Delta Nb = Nb - (0.70 \times 7.74C)$ Dual stabilized steels

Results and discussion

Microstructural analysis

Microstructural cubes of the ferritic stainless steels are presented in Figure 1. The microstructure for all grades studied was homogeneous and constituted of recrystallized grains.

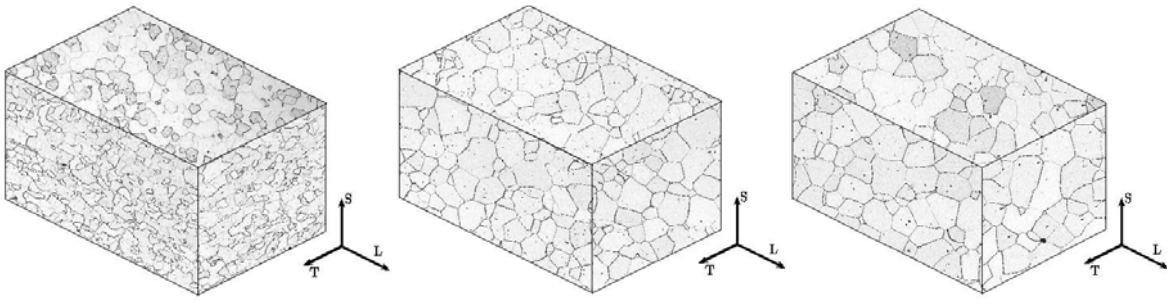

Figure 1. Optical microstructural cube of the ferritic stainless steels, Villela's reagent. 200X.

Grain size was 16,5µm (AISI 439); 49,4µm (ACE P439A) and 64,3µm (AISI 441). This difference is related to the steel fabrication standard condition, as heat treatment and chemical composition. More niobium content, mainly ΔNb, increases the recrystallization temperature and so the steel annealing must be done at higher temperature and time, which allows the grain growth.

Tensile tests

Tensile tests were carried out in several temperatures with sub-size specimens. Yield strength and ultimate tensile strength versus temperature are presented in Figure 2.

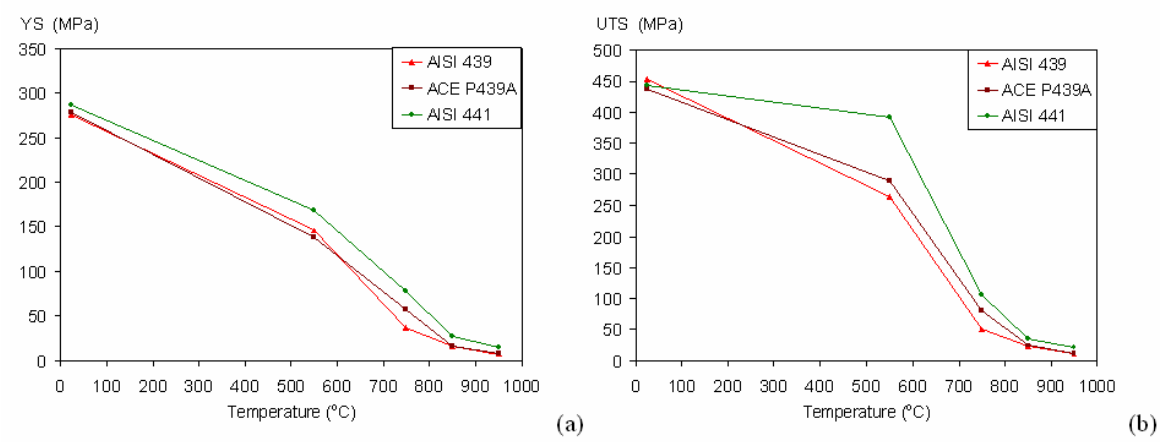

Figure 2. Results of tensile tests at different temperatures. Yield strength (a) and Ultimate tensile strength (b).

Ferritic stainless steels have shown a strong decrease of mechanical properties in function of the temperature. This behavior is more observed for UTS around 550 and 750ºC. A same mechanical behavior was observed for the 3 studied grades up to 300ºC. AISI 441 has presented higher yield and ultimate tensile strength than the other grades for the temperatures above 500°C. ACE 439A presents an intermediate behavior. This result shows the important effect of niobium on high temperature mechanical properties, mainly as found in solid solution (ΔNb). A lowest interstitial content (C+N) and highest solid solution free niobium allows the precipitation of Laves phase (Fe_2Nb) and an increase of the yield and ultimate tensile strength.[2]

Creep resistance Tests

Figure 3 presents the results of the creep test "SAG TEST" at 850 and 950ºC. The higher the value of deflection, the greater the material deformation is and consecutively the less its creep resistance is.

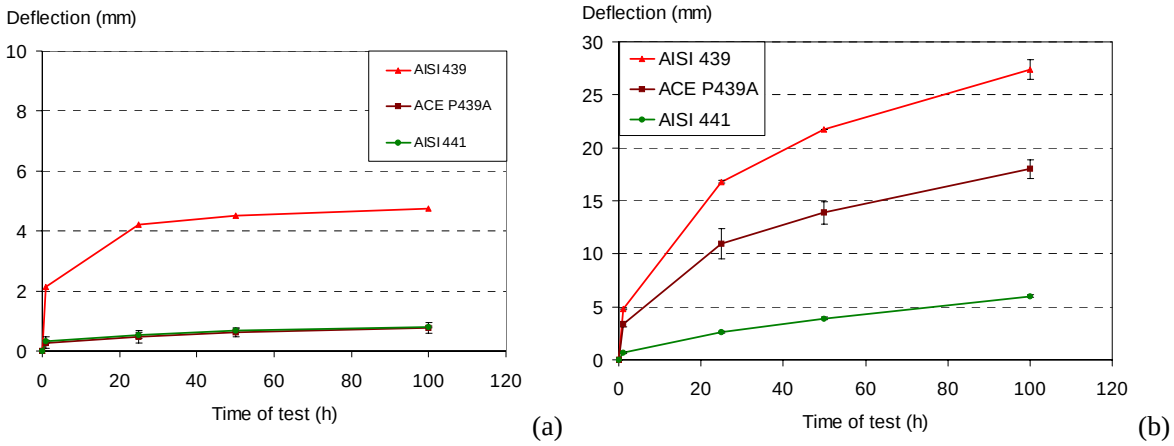

Figure 3. Results of the creep test. (a) 850ºC and (b) 950ºC.

The grades have presented a significant difference of creep resistance at the two temperatures. At 850ºC, the steels studied have presented a very small deformation (always less than 5mm). AISI 41 and ACE P439A, with high ΔNb, have presented a negligible deformation and an excellent creep resistance. At 950ºC, the grades have presented a significant deformation, mainly the AISI 439. AISI 441 presents the best creep behavior. It was observed that titanium has not presented a significant effect on the creep resistance. On the other hand, it was verified that the

main effect of niobium was found considering free niobium in solid solution (ΔNb) and not its total amount. Figure 4 presents microstructural examinations for both temperatures.

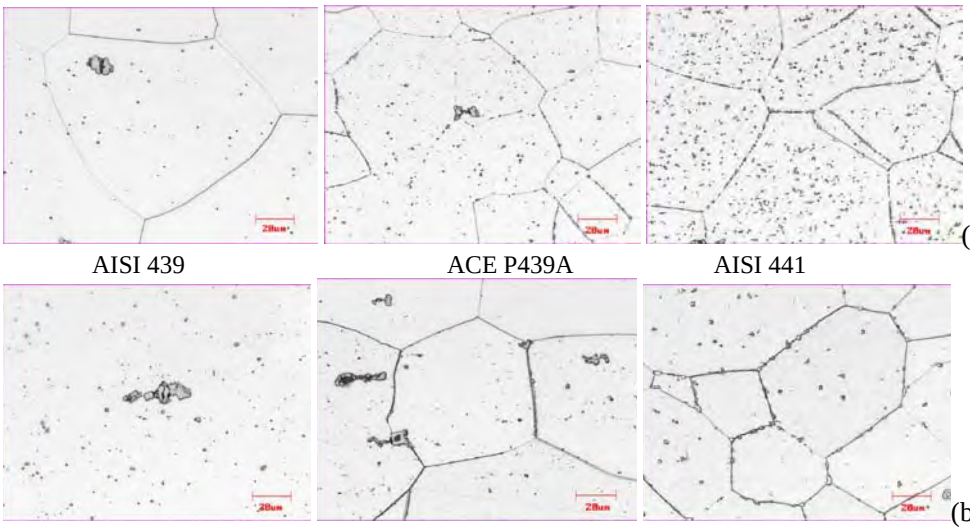

Figure 4. Microstructural analysis of the creep test samples. (a) 850ºC and (b) 950ºC.

As observed, a microstructural evolution exists with the increase of the temperature in the creep test, which has justified the different steel behavior at these temperatures. This microstructural evolution can be explained by grain growth and dissolution /coarsening of niobium rich phases. Figure 5 presents the result of grain size measurement of the steels after creep tests at the two temperatures (100 hours) and makes a comparison with the initial grain size of the samples.

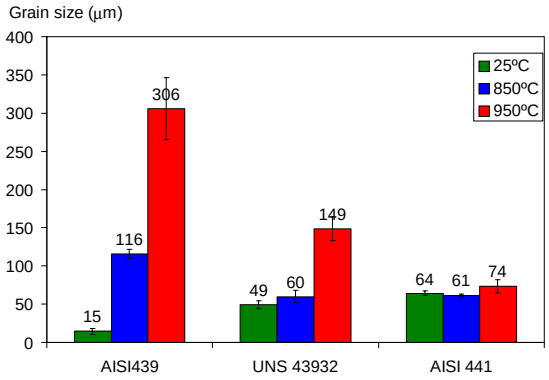

Figure 5. Evolution of the grain size during SAG TEST – time 100h.

As observed in Figures 4 and 5, the evolution of grain size in function of the temperature is directly related to the chemical composition of the grades. Moreover, it is verified that the main alteration of grain size was obtained at 950ºC in relation to the condition before the test, except for the titanium mono-stabilized steel (AISI 439). At 850ºC, niobium stabilized steels have not presented significant variation at the grain size, while AISI 439 has shown a significant increase. ACE P439A and AISI441 present precipitation of niobium rich phases in the bulk and grain boundaries. In the case of grain boundaries, these precipitates have a pinning action and inhibit the grain growth.[1,10] At 950ºC, a lesser niobium amount precipitates in the bulk and grain boundaries, indicating that they were dissolved at this temperature and explaining its grain growth, excepted to AISI 441. AISI 439 has continued to present a superior grain growth.

The dissolution technique of steels was carried out for chemical extraction of precipitates from SAG TEST specimens and SEM and X-Ray difractometer was used. Figure 6 presents SEM analysis of the precipitates obtained by dissolution technique.

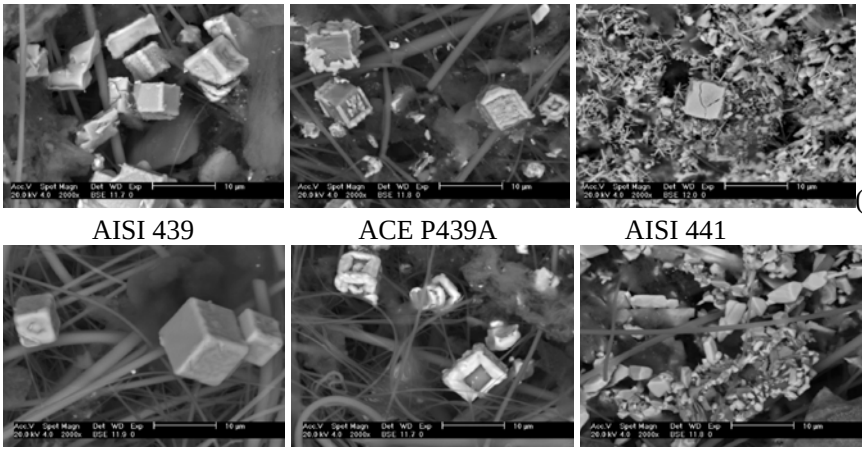

Figure 6. Analysis in SEM of precipitates obtained by the steel dissolution in creep samples. (a) 850ºC; (b) 950ºC.

AISI 439 has presented TiN and TiC precipitates at the two temperatures. TiN precipitates present a cube shape while TiC one is found on the extremities of the cube diagonal axis. ACE 439A with intermediate titanium and niobium contents has presented TiN precipitates, but without TiC presence on the extremities. The fine precipitates observed at the metallographical analysis (Figure 4) were identified as "Laves phase" of Fe_2Ti and Fe_2Nb type at 850ºC. Nb(C, N) have precipitated around TiN. At 950ºC, the dissolution of Laves phase and coalescence of Nb(C, N) have occurred. The main difference found between AISI 441, and ACE P439A, is the presence of Fe_5Nb_3 precipitates in the grain boundaries. As observed in Figure 6(d), Fe_5Nb_3 precipitates have a circular shape and are presented continuously (joined together). It was verified that ferritic stainless steel creep resistance is directly related to chemical composition, while grain size has little significant effect on its improvement.

Low cycle fatigue (LCF) tests

LCF tests were carried out under strain control at two temperatures (300 and 850ºC). Specimens were obtained from “plates” (28.00mm thick) Figure 7 shows the LCF lifetime result for both temperatures.

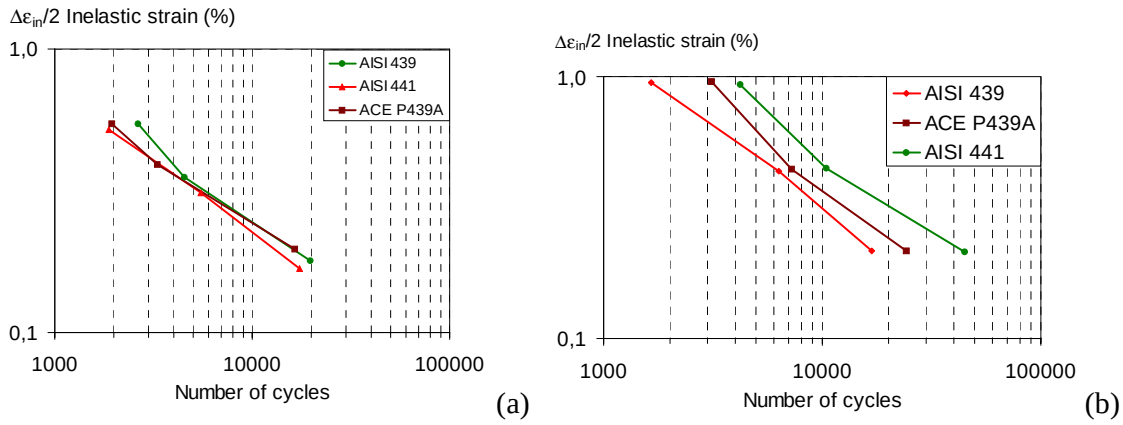

Figure 7. LCF lifetime of the ferritic stainless steels – cycle N= 100. Temperature: 300ºC (a) and 850ºC (b).

Ferritic stainless steel has presented a similar mechanical behavior and fatigue lifetime at 300ºC. At 850ºC, ACE P439A has an intermediate behavior and AISI 441 has the best performance. Higher chromium content and, mainly, niobium free in solid solution (ΔNb) as observed at creep tests contribute to the increase of LCF lifetime at high temperature.

Comparison of industrial performance between AISI 441 and ACE P439A

As the majority of ferritic stainless steels have been used in tube shape in the exhaust system, a comparison of HF welding performance was done, as shown on Figure 8.

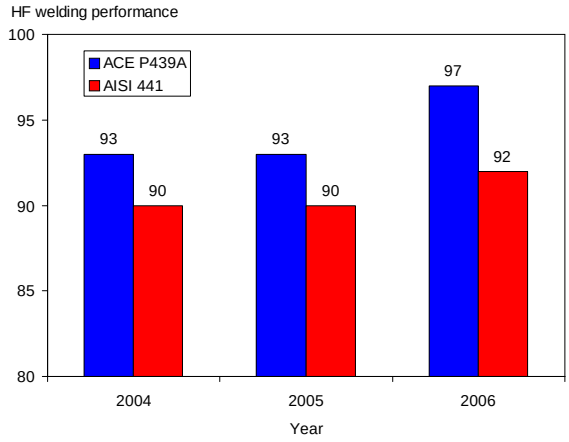

Figure 8. Comparison of HF tube welding performance of ACE P439A and AISI 441.

ACE P439A has better HF tube welding performance than AISI 441. Moreover, an evolution of this performance has been observed because ACE P439A production's volume has been increasing during the years. It is important to emphasize that the ACE P439A performance concerns its better forming condition (chemical composition and mechanical properties) and lower tube complexity (temperature, upset, process speed, scarfing). In addition, ACE P439A has presented some advantages of industrial production; its slab cost is lower than AISI 441 by at least 5%.

Conclusions

The main conclusions are:

- ACE P439A presents good mechanical properties (creep, low cycle fatigue and tensile test), which are better than AISI 439 for temperatures above 650°C. Its mechanical properties are quite similar to AISI 441 up to 850°C. Above this temperature, the use of AISI 441 is recommended. The results show an important effect of niobium on the high temperature mechanical properties.
- ACE P439A, as compared to AISI 441, presents better conditions of fabrication, such as tube welding and forming (drawability), lower cost and higher productive scale.
- According to this study, ACE P439A can be used in the hot part of the exhaust system, including manifold application.

References

[1] SCHMITT, J.H. "Some examples of stainless steel use in the automotive industry." Key Engineering Materials. v. 230-232, 2002, p. 17-22.

[2] FUJITA, N.; OHMURA, K.; KIKUCHI, M.; SUZUKI, T.; FUNAKI, S.; HIROSHIGE, I. “Effect of Nb on high-temperature properties for ferritic stainless steel” Scripta Materialia, v.35, n. 6, 1996, p. 705-710.

[3] ALVES, H. J. B., MANTEL, M. CARVALHO, J.A.N. AQUINO, M.V. “Development of ferritic stainless steels for automotive exhaust systems”. In: 4TH EUROPEAN STAINLESS STEEL. Paris, France. 2002.

[4] SCHIMITT, J.H.; CHASSAGNE, F.; MITHIEUX, J.D. « Some recent trends in niobium ferritic stainless steels.” In: Recent advances of niobium containing materials in Europe. HULKA, K.; KLINKENBERG, C.; MOHRBACHER, H. Düsseldorf, Germany: Verlag Stahleisen GmbH, p. 134-148. 2005.

[5] DAVIS, J. R. “Stainless Steels.” Materials Park, ASM International Handbook Comitee, 1994, p. 3-5 and 445 - 446.

[6] JOHNSON, J. N. “Influence of columbium on the 870oC creep properties of 18% chromium ferritic stainless steels.” In: SAE TECHNICAL PAPER SERIES 810035 INTERNATIONAL CONGRESS AND EXPOSITION. Cobo Hall, Detroit, Michigan. February 23-27, 1981.

[7] MUGHRABI, H; CHRIST, H.J. “Cyclic deformation and fatigue of selected ferritic and austenitic steels: specific aspects.” ISIJ International, v.37, No. 12, 1997, p. 1154-1169.

[8] SATO, E.; TANOUE, T. “Present and Future Trends of Materials for Automotive Exhaust System.” Nippon Steel Technical Report No. 64, January 1995. p. 13-19.

[9] FUJIMURA, H.; TSUGE, S. “Effect of C, Ti, Nb on recrystallization behavior after hot deformation in 16%Cr ferritic stainless steel.” In: The Fourth International Conference on Recrystallization and Related Phenomena. The Japan Institute of Metals, 1999, p. 763-768.

[10] MANTEL, M.; BAROUX, B.; GEX, D.; PEDARRÉ, P. “The effect of niobium on the recrystallization of 17%Cr. Recrystallization’90.” The Mineral, Metals & Materials Society, 1990.

TAILORED STRIPS – A COST AND WEIGHT SAVING PROSPECT FOR AUTOMOTIVE EXHAUST SYSTEMS

S. Schuberth[1], I. Schael[1], H.-P. Vogt[2]

[1]ThyssenKrupp Nirosta GmbH, Germany, [2]ThyssenKrupp Tailored Blanks, Germany

Abstract

Continuous developments for reducing automotive emissions have enhanced the requirements regarding design and construction of exhaust systems. Increasing exhaust temperatures due to highly efficient engines and further developed catalytic converters, some including DPF (diesel particulate filters) or SCR (selective catalytic reduction), demand materials with extended corrosion resistance in order to fulfil the long-term guarantees given by car manufacturers. Another important facet of emission reduction is the necessity to lower weight.

Stainless steel tailored strip has the potential to allow for these needs. By combining different steel grades it becomes possible to apply expensive, highly corrosion resistant materials only to parts where they are actually necessary. Furthermore, a combination of different gauges saves weight in parts which are less mechanically stressed.

Introduction

Today's automotive exhaust systems are to a very large extent built exclusively out of stainless steels. The high requirements on the employed materials are ascribed to various reasons. The different parts of an exhaust system are exposed to site-specific temperature ranges, mechanical loading and corrosion conditions, dependent on their position in the exhaust line. Also the material demands concerning formability and weldability are differing.

Consequently we find a wide palette of stainless steels which are currently applied in automotive exhaust systems. Chemical compositions and typical mechanical properties of such steels are listed in Tables 1 and 2.

Table 1. Chemical composition of stainless steels for exhaust systems

Steel grade	Chemical composition [%]						
	C	Cr	Mo	Ni	N	Ti	Nb
1.4512	0,015	11,5	-	-	0,015	0,20	-
1.4510	0,020	16,5	-	-	0,015	0,45	-
1.4509	0,020	17,5	-	-	0,015	0,15	0,40
1.4113	0,045	16,5	1,0	-	0,030	-	-
1.4513	0,020	17,0	1,0	-	0,015	0,45	-
1.4607	0,020	19,0	-	-	0,020	0,15	0,40
1.4521	0,020	17,5	2,0	-	0,020	0,20	0,25
1.4301	0,040	18,0	-	8,0	0,050	-	-
1.4401	0,030	16,5	2,0	10,5	0,040	-	-
1.4541	0,030	17,0	-	9,0	0,020	0,30	-
1.4550	0,030	17,0	-	9,0	0,020	-	0,35
1.4571	0,030	16,5	2,0	10,5	0,020	0,30	-
1.4828*	0,050	19,0	-	11,0	0,050	-	-
1.4835**	0,080	21,0	-	11,0	0,150	-	-

* contains 1.9% Si

** contains 1.8% Si, contains Cer

Table 2. Typical mechanical properties of stainless steels for exhaust systems

Steel grade	Yield stress $R_{p0,2}$ [MPa]	Tensile strength R_m [MPa]	Total elongation A_{80} [%]
1.4512	275	430	33
1.4510	290	450	32
1.4509	320	480	32
1.4113	350	550	24
1.4513	320	480	31
1.4607	320	480	31
1.4521	340	510	29
1.4301	300	630	57
1.4401	300	620	55
1.4541	280	615	57
1.4550	280	615	57
1.4571	290	605	56
1.4828	300	640	57
1.4835	370	720	50

The requirements on the applied steel grades continue to increase. New motor concepts e. g. led to higher temperatures in the exhaust line. Demands for extended life cycle guarantees entail increasing corrosion resistance. Figure 1 gives an overview of stainless steels which are fit for application at elevated temperatures and/or under special wet corrosion conditions.

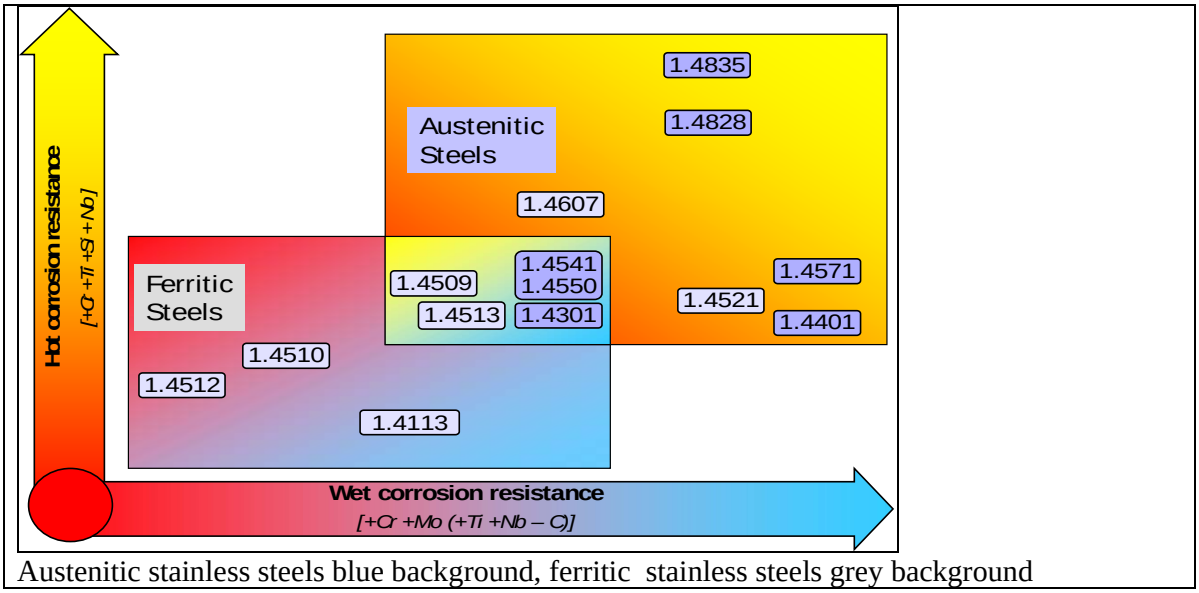

Austenitic stainless steels blue background, ferritic stainless steels grey background

Figure 1. Hot corrosion and wet-corrosion resistant stainless steels

The here discussed increasing material requirements come along with the necessity to noticeably reduce costs. The price of stainless steel is strongly determined by the price development of its alloying constituents. Especially austenitic stainless steels are predominantly influenced by the price of nickel. The enormous increase of the nickel price in the last years (Figure 2) has brought on the call for substituting these steels by ferritic stainless steels.

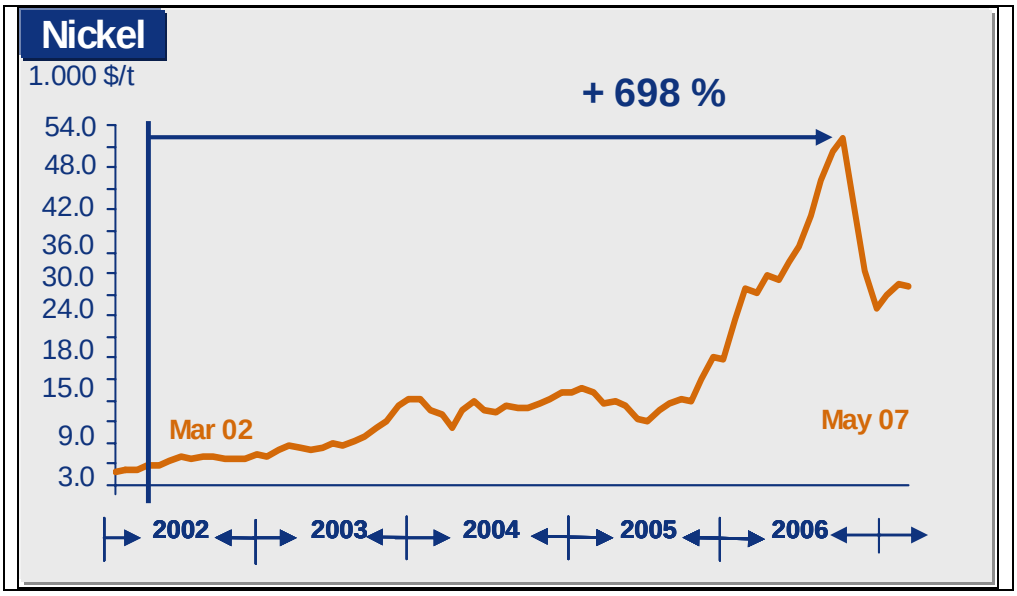

Figure 2. Recent development of the nickel-price

Helpful is the development of new corrosion and heat resistant ferritic stainless steels, e. g. NIROSTA® 4607. But as austenitic stainless steels cannot be substituted completely it is equally important to find better solutions for combining austenitic and ferritic grades.

Tailored strips present such a solution. This technology allows a combination of austenitic and ferritic grades already in the primary material. Therewith it becomes possible to reduce the application of austenitic grades to a targeted, actually needed minimum. Furthermore steel strips of different thicknesses can be joined together which results in another price advantage. Besides this weight can be reduced if strip elements are placed in accordance with the main loading direction. 20-40 % of weight may actually be reduced.

Processing of Tailored Strips

An alternative for the production of profiles or other formed parts is offered by ThyssenKrupp Tailored Strips®. Especially exhaust system parts or bead seat rings for car wheels may be processed from coiled stainless steel strip which from the beginning has been designed in accordance with the requirements of the later part [3]. Coil weights can amount to 15 metric tonnes. A worldwide unique unit developed by ThyssenKrupp Tailored Blanks is able to join stainless steels of different grade, finish and gauge with a continuous, several hundred meters long weld. Combinations of stainless steels with carbon steels are also possible. Two or three slit strips can be joined together (Figures 3 and 4). Tailored strips are an advancement of tailored blanks which have been on the market for several years, but are limited to a blank length of 3 meters [1].

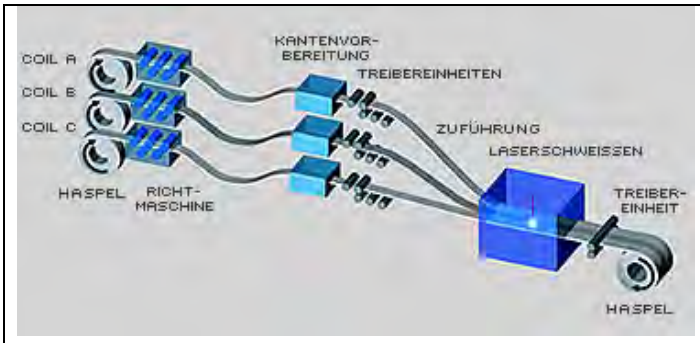

Figure 3. Production unit [3]

Figure 4. Continuous laser welding [3]

Production of ThyssenKrupp Tailored Strips®:

- uncoiling and levelling of strips,
- preparation of the edges for high welding velocities,
- laser-welding of 3 strips in one production step,
- 100 % weld inspection by QA system,
- marking of defects,
- coiling or cutting-to-length at the run-out.

Delivery forms:

Different delivery forms are possible ranging from sheet to coiled strip. In the process chain profiles are shaped by sending a narrow, slit stainless steel strip through a trueing line with several sets of rolls arranged in series. The required cross-section is therewith created. The user can obtain a stainless steel product which in delivery condition is already fit for the future impacts on the intended part. Reinforcements for highly loaded regions are not necessary. The user can skip complete production steps and saves weight, costs and time for the remaining production process. (Figure 5). He can also, as far as this product is concerned, do without parts of his plant, and can thus realize a higher degree of automation in a continuous process [4].

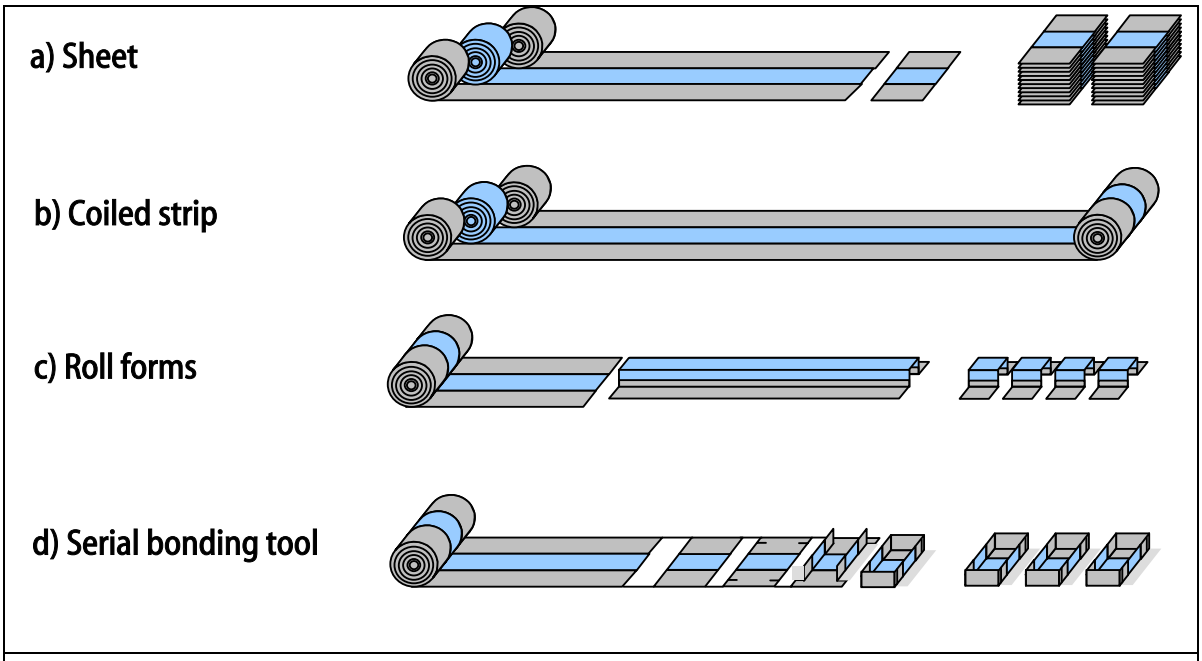

Figure 5. Processing of stainless steel tailored strips [4]

The production of steel strip with a continuous laser weld was until lately regarded as impossible. The technical limit was a weld length of 3 meters which led to the production of tailored blanks provided that the individual sheets were at least 200 mm in width.

The problem: During laser welding the beam melts the edges of the strips. With increasing weld length the strips heat up which leads to warping and a widening of the weld gap. For a correct laser weld the gap has not to be wider than 0.08 mm as weld defects would result. This was actually the greatest technical challenge. The problem was solved at ThyssenKrupp Tailored Blanks in Gelsenkirchen by installing a newly developed system for cooling the weld. Furthermore the fixed welding head is swivel-mounted and can be tilted by 5 mm so that irregularities of the welding gap will be compensated [4].

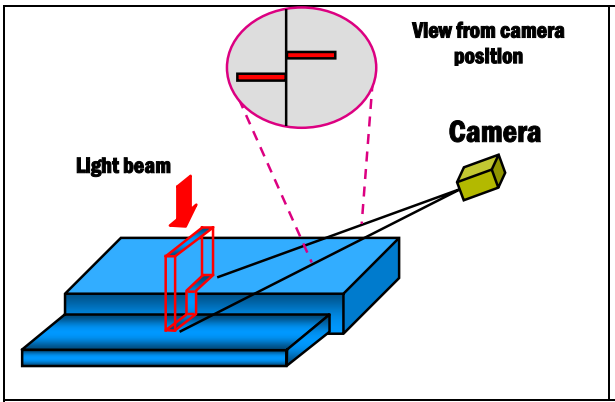

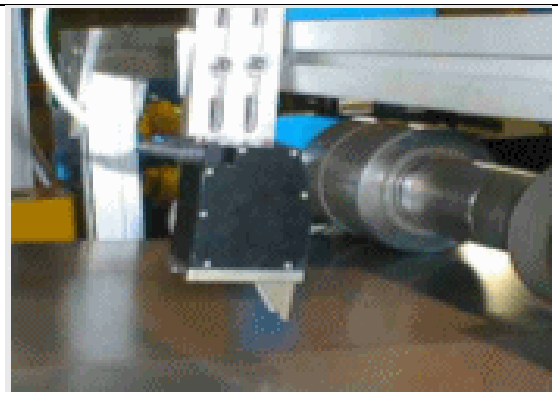

Figures 6 and 7. Detection of misaligning edges and fallen in seams [4]

In order to minimise such irregularities the steel strips are levelled before they are entered into the welding line. Besides this the edges of the original material should be prepared for welding by paring, milling or realigning which is one of the technical challenges for tailored strips production solved at ThyssenKrupp Tailored Blanks®. Asymmetrical strip length is another

technical defiance when it comes to coiling of the tailored steel strips and yet another technical break through achieved in recent years. The weld is controlled by 100 % (Figures 6 and 7). Misaligning edges and fallen in seams are permanently monitored with a camera system. A hole detecting system identifies, marks and discharges defect material (Figures 8 and 9). Respective documentation is consistently carried out from the first to the last meter.

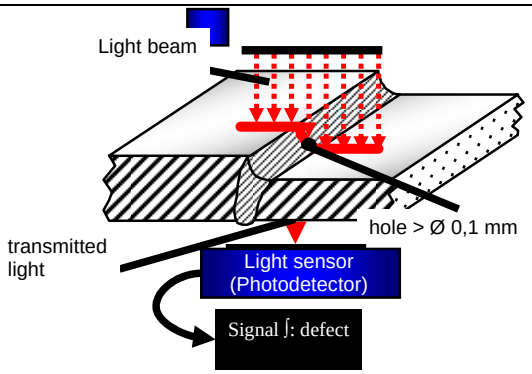

Figures 8 and 9. Detection of holes and not completely welded areas [4]

Try-out

The relatively new tailored strips technique has already been thoroughly tested in parts. Eberspächer GmbH & Co KG has produced deep-drawn half shells for a series-production silencer with tailored strips in a large-scale test. Beforehand a finite-element simulation of the tool and the work piece had been performed for the application of tailored strips. The production of the optimised part was first tested in a hydraulic press. After the half shells were able to be produced without cracking, production was then carried out in a transfer press under series-production conditions. (Figures 10 and 11). Comparison of the simulation results and the actual part showed very good compliance regarding seam and thickness. The thickness of the real part in Grade 1.4301 was continuously 1.2 mm. By employing tailored strips thickness could in some ranges be reduced to 0.7 mm. The advantages of different material combinations due to weight reduction amounted to 15–40 % of the series-produced part [2]. The cost advantage on behalf of thickness reduction is already considerable. If one succeeds in producing the half shells by applying cost-saving ferritic stainless steel grades such as NIROSTA® 4607 in combination with austenitic stainless steels, further cost optimisation would become possible.

Conclusions

Tailored strips are especially suited for stainless steel applications. The strips which are carefully designed for the demands of further production lead to weight reduction of future parts, thereby

Figures 10 and 11. Exhaust system half shell in Grade 1.4301 before and after welding. Segments of 112 mm with t = 1.2 mm, 336 mm with t = 0.7 mm and 97 mm with t = 1.2 mm [2]

already lowering costs. By then combining low-cost ferritic stainless steel grades, e. g. for parts requiring corrosion resistance but less formability, with highly formable austenitic grades a substantial cost reduction can be achieved. Further production steps can be integrated or skipped resulting in a shortening of production chains.

References

[1] C. Dohr; A., Brunsbach: „ThyssenKrupp Tailored Strips® – kontinuierliches Laserschweißen von Spaltbändern für die Automobilindustrie" ThyssenKrupp techforum, 7/2005, pp. 10- 13

[2] S. Junk; T. Grün: „Innovativer Leichtbau in der Abgastechnik, Einsatz von Tailored Strips reduziert Gewicht und Kosten", ATZ 04/2007, Jahrgang 109, p. 2 – 7

[3] ThyssenKrupp Tailored Blanks: „Tailored Blanks- Die lokale Verstärkung", Datenblatt ThyssenKrupp Tailored Blanks GmbH, Duisburg, 2007

[4] H.-P. Vogt:: "ThyssenKrupp Tailored Strips® - Eine Möglichkeit zur Optimierung der Anwendungen von Stahl und Edelstahl", Presentation at „Tagung des Automotive Circle International: European Automotive Laser Application (EALA), Bad Nauheim, 2008

THERMAL FATIGUE BEHAVIOR OF FERRITIC STAINLESS STEEL FOR AUTOMOTIVE EXHAUST SYSTEM

J. Hamada[1], H. Kajimura [1], N. Morihiro[2]

[1]Nippon Steel & Sumikin Stainless Steel Corp., Japan, [2]Hikari Stainless Steel Technology, Japan

Abstract

The exhaust manifold of an automobile is exposed to thermal cycles by high temperature exhaust gas. Thermal fatigue resistance is one of the most important properties for an automotive exhaust manifold. In this study, we investigated changes in the microstructure, the crack propagation and the hysteresis loop during the thermal fatigue of Type 429 ferritic stainless steel. In addition, we compared Type 429 and Type 444 in order to evaluate the effect of high temperature strength on the thermal fatigue life. The following results were obtained.
(1) During the thermal fatigue process, some wrinkles occurred on the surface of the material, and some cracks progressed in the direction of thickness.
(2) During the thermal fatigue process of Type 429 in the temperature range from 200°C to 800°C, the material was softened by the reduction of the amount of solute Nb, and the dynamic recovery and recrystallization.
(3) The form of hysteresis loop changed with the increase in cycles. By considering the softening of the material by heat treatment, the change in the form could be predicted to some extent.
(4) Type 444 with high temperature strength had a longer thermal fatigue life than Type 429. The thermal fatigue behavior and life were related to high temperature strength, and increase in high temperature strength was effective in improving the thermal fatigue life.

Introduction

Ferritic stainless steels containing Nb, Si, Mo, etc. are applied to heat-resistant materials such as automotive exhaust system parts, since they excel in high temperature strength, oxidation resistance and formability. In particular, thermal fatigue resistance is required for materials in the exhaust system because of the heating and cooling cycles caused by the exhaust gas.[1,2] Heat-resistant ferritic stainless steels with excellent thermal fatigue characteristics have been developed mainly for high temperature strength improvement.[3-12] Several studies have determined the criterions of thermal fatigue lifetime of ferritic stainless steel as exhaust manifolds.[13-15] However, there are few reports on the behavior during the thermal fatigue process.[16] In this study, we investigated the changes in the microstructure, the crack propagation and the hysteresis loop during thermal fatigue of Type 429 (13%Cr-0.9%Si-0.5%Nb-LowC,N), typical heat-resistant ferritic stainless steel. We also compared Type 429 and Type 444 (18%Cr-1.8%Mo-0.5%Nb-0.1%Ti-LowC,N) was performed in order to evaluate the effect of high temperature strength on the thermal fatigue life.

Experimental procedure

Typical chemical compositions of the steels used in this work are listed in Table 1. New thermal fatigue testing using the pipe specimen (ϕ38.1×2 mmt) was conducted with a controlled restriction ratio by the servo-hydraulic testing machine and a temperature profile by the heating and cooling system assisted by computer.[2] The specimen was heated from outside with a high frequency induction heating system, and cooled by output control and by ventilation from the pipe inside. The temperature and the axial strain of the specimen were synchronized so that the axial restriction ratio (η) became constant during the heat cycle. Thermal fatigue tests of Type 429 were carried out in the temperature range from 200°C to 800°C. The examination was interrupted before the lifetime expired and it was considered to be an interrupted specimen. The changes in the microstructure, crack generation and the hysteresis loop in the interrupted and failed specimens of Type 429 were examined. In addition, in order to investigate the effect of high temperature strength on the thermal fatigue life, comparative examinations of Type 429 and Type 444 were performed in the temperature range from 200°C to 750°C. The life cycle was determined by the period of crack penetration. Microstructural observations of the specimens were carried out by optical microscope, transmission electron microscopy (TEM) and electron back-scattering pattern (EBSP). The amount and kind of precipitates were evaluated by electrolytic extraction residue and X-ray diffraction, respectively. Then, the section hardness of the specimens was measured. Furthermore, the tensile tests of the sheet specimens (2 mmt) with and without aging at 800°C for 100 h were carried out at the elevated temperature.

Tabel.1. Chemical compositions of steels used (mass %).

Steel	C	Si	Mn	P	S	Ni	Cr	Mo	Nb	Ti	N
Type 429	0.004	0.86	0.24	0.02	0.001	0.08	13.3	0.01	0.47	0.005	0.008
Type 444	0.005	0.35	0.99	0.03	0.001	0.10	18.4	1.8	0.48	0.10	0.012

Results and discussions

Microstructure and crack during thermal fatigue

Figure 1 shows the change in the maximum tensile and compression stress in the thermal fatigue experiment of Type 429 in the temperature range from 200°C to 800°C and with a restriction ratio of 50%. In this experiment the thermal fatigue life was 1202 cycles. The maximum tensile and compression stress gradually decreased with the increase in the cycles, and repetition softening occurred under this condition. Figure 2 shows the microstructures and the cracks of the interrupted specimen of Type 429.

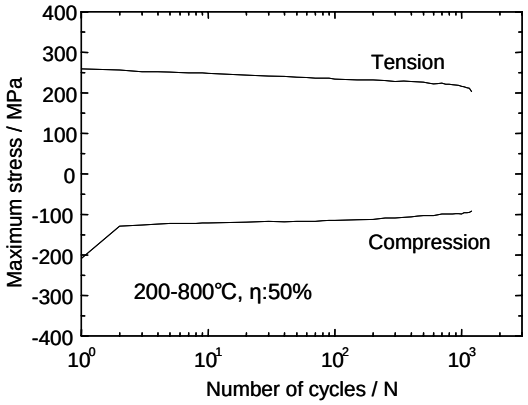

Figure 1. Change in the maximum tensile and compression stress.

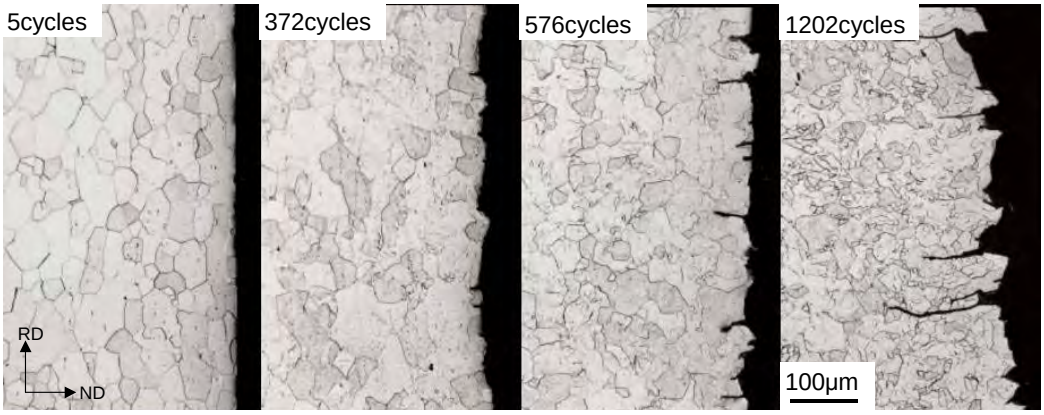

Figure 2. Microstructures and cracks of interrupted specimen(T_{min}:200°C - T_{max}:800°C, η:50%).

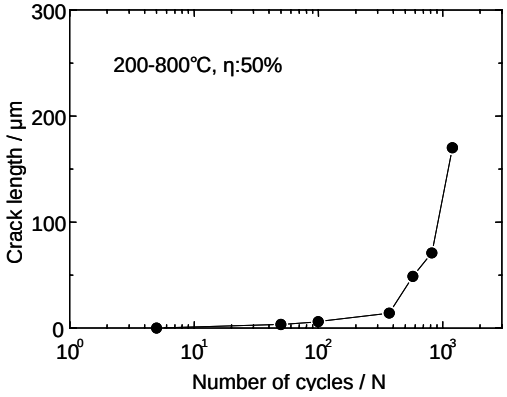

Figure 3. Crack length of the interrupted specimen.

During this thermal fatigue test, some wrinkles were observed on the surface of the material at about 300 cycles, and some cracks progressed in the direction of thickness. In addition, fine grains formed especially near the cracks with the increase in the cycles. The crack length of each cycle was evaluated by the average value of the longest five cracks as shown in Figure 3. The growth rate of a crack became higher after 372 cycles. Figure 4 shows orientation imaging micrographs of the interrupted specimen by EBSP. The mapping of ND was measured from TD at 1 μm steps. The black lines indicate the high-angle boundaries with misorientations of more than 15 degrees, while the gray lines indicate the low-angle boundaries with misorientations of less than 15 degrees. Although most crystal grain boundaries were high-angle boundaries after 5 cycles, low angle boundaries formed in the inside grain after 372 cycles. Fine crystal grains with high-angle boundaries were observed after 576 cycles that crack growth promoted. The finer grain structure was obtained in the final specimen. These results suggest that the dynamic recovery and recrystallization occur during thermal fatigue.

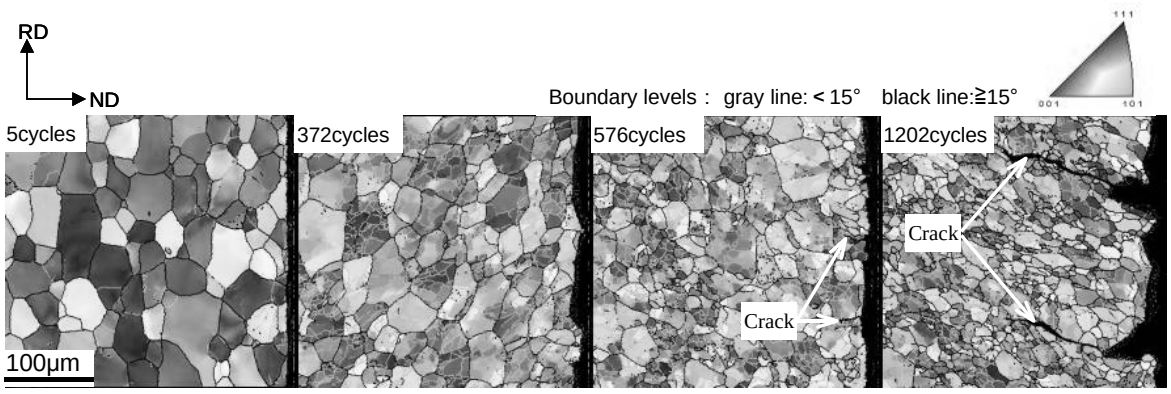

Figure 4. OIM maps of interrupted specimen(T_{min}:200°C - T_{max}:800°C, η:50%).

Figure 5 shows an example of TEM observations. The precipitates were identified as Nb(C,N), Fe_2Nb and M_6C by X-ray diffraction analysis of the electrolytic extraction residue. The precipitation of Nb was saturated after about 100 cycles. Although slight coarsening of precipitates was observed with the increase in the cycles, the precipitates were dispersed within the grain and dislocations were entangled with precipitates. Figure 6 shows the cross-sectional hardness of the thermal fatigue specimen at room temperature. With the increase in the cycles, the softening was also found in this figure as well as in Figure 1. The reduction of the amount of solute Nb and the dynamic recovery and recrystallization by the heat cycle are presumably related to the softening phenomenon during the thermal fatigue process.

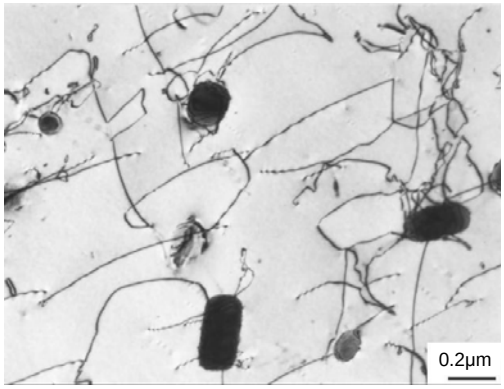

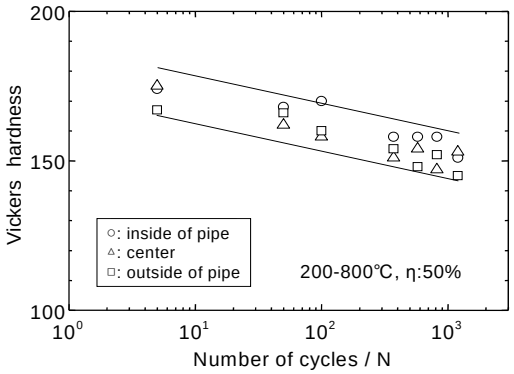

Figure 5. TEM micrograph of interrupted specimen after 819 cycles (T_{min}:200°C - T_{max}:800°C, η:50%).

Hysteresis loop during thermal fatigue

Figure 7 shows several examples of the stress-strain hysteresis loop during the thermal fatigue test of Type 429 in the temperature range from 200°C to 800°C and with a restriction ratio of 50%. During the thermal fatigue process, the hysteresis loop of the stress and strain changed little-by-little with the increase in the cycles. This phenomenon is due to the softening of the material during thermal fatigue. The hysteresis loop was estimated under the test conditions (temperature range, restriction ratio) and the material physical properties (thermal expansion coefficient, proof stress and Youngs modulus at elevated temperature).[16] Figure 8 shows the calculated hysteresis loop using both the physical properties of the material with and without aging. Although the calculated shapes of the hysteresis loop were slightly different from the measured shapes, the changes in the shape in the thermal fatigue test were simulated by

considering the softening of the material by heat treatment. The changes in the hysteresis loop were caused by the changes in the physical properties during the thermal fatigue test.

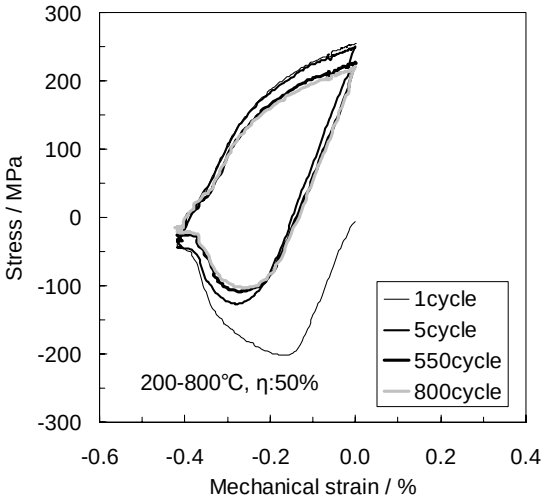

Figure 7. Hysteresis loops in thermal fatigue test.

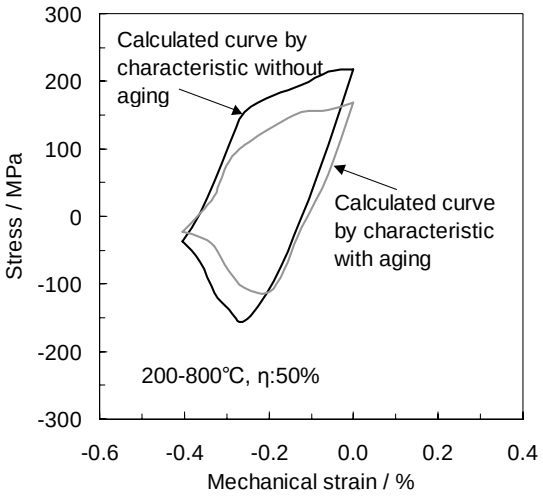

Figure 8. Calculated hysteresis loops.

Comparison of thermal fatigue life of Type 429 and Type 444

Figure 9 shows the relation between the thermal fatigue life and the inelastic strain range on Type 429 and Type 444 in the temperature range from 200°C to 750°C and with a restriction ratio of 50% and 70%. Each line in Figure 9 is the estimated result by applying the Coffin-Manson equation for the thermal fatigue life of each material.[17,18] The inelastic strain ranges in the thermal fatigue test of Type 444 were smaller than those of Type 429, and Type 444 had a longer thermal fatigue life than Type 429. Figure 10 shows the comparison of tensile strength of Type 429 and Type 444 sheets at the elevated temperature. Type 444 had higher tensile strength compared with Type 429. It was presumed that the increasing in high temperature strength by Mo addition prevented softening and improved the thermal fatigue life. It was concluded that the thermal fatigue behavior and life were related to the high temperature strength of materials, and increasing in high temperature strength is effective in improving thermal fatigue life.

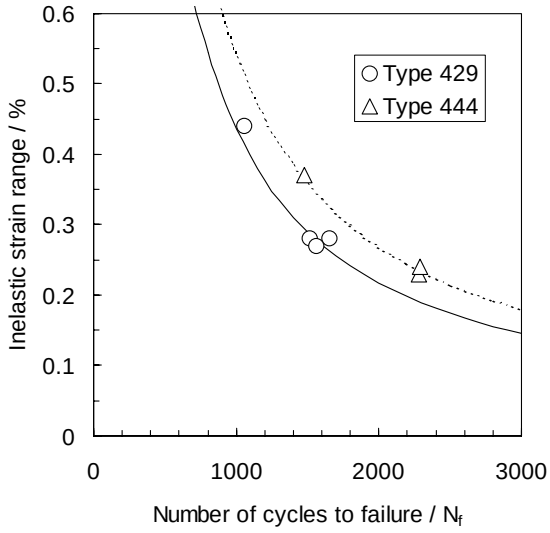

Figure 9 Comparison of thermal fatigue life of Type 429 and Type 444 (T_{min}:200°C - T_{max}:750°C, η:50 and 70%).

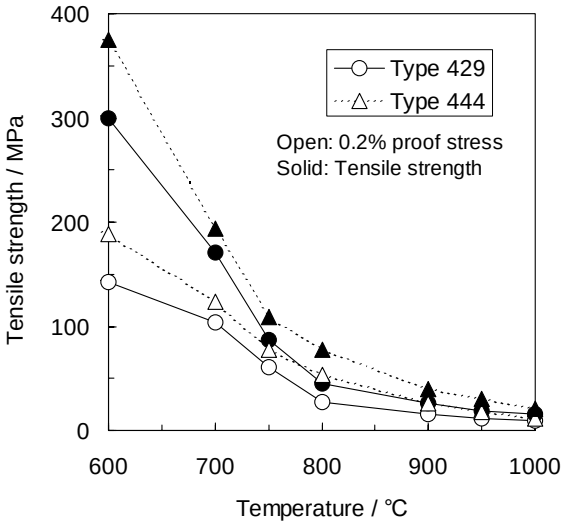

Figure 10. High temperature tensile properties of Type 429 and Type 444 sheets.

Conclusions

The changes in the microstructure, the crack propagation and the hysteresis loop of the stress and strain during thermal fatigue of Type 429 ferritic stainless steel were investigated. Comparative examination of Type 429 and Type 444 was also performed in order to evaluate the effect of high temperature strength on the thermal fatigue life. The main results are as follows.

- During the thermal fatigue process, some wrinkles occurred on the surface of the material, and some cracks progressed in the direction of thickness.
- During the thermal fatigue process of Type 429 in the temperature range from 200°C to 800°C, the material was softened by the reduction of the amount of solute Nb, and the dynamic recovery and recrystallization.
- The form of the hysteresis loop changed with the increase in cycles. By considering the softening of the material by heat treatment, the change in the hysteresis loop could be predicted to some extent.
- As a result of comparing the thermal fatigue life of Type 429 with Type 444, Type 444 with high temperature strength was found to have a longer thermal fatigue life than Type 429. The thermal fatigue behavior and life were related to high temperature strength, and the increase in high temperature strength was effective in improving the thermal fatigue life.

References

[1] H. Kajimura: Bull. Iron Steel Inst. Jpn., 11, 2006, pp.67-73.
[2] M. Miyahara, H. Kajimura and K. Higuchi: Proc. of High Temperature Properties of Stainless Steel and Applications for Automobile Exhaust System, ISIJ, Tokyo, 2003, pp.10-15.
[3] N. Fujita, K. Ohmura, M. Kikuchi, T. Suzuki, S. Funaki and I. Hiroshige: Scr. Mater., 35, 1996, pp.705-710.
[4] N. Fujita, K. Ohmura, E. Sato and A. Yamamoto: Shinnittetsu Giho, 361, 1996, pp.20-24.
[5] N. Fujita: Shinnittetsu Giho, 371, 1999, pp.30-34.
[6] Y. Inoue and M. Kikuchi: Shinnittetsu Giho, 378, 2003, pp.55-61.
[7] Y. Tarutani, M. Miyahara, T. Hashizume, K. Higuchi and H. Fujikawa: Sumitomo Metals, 45, 1993, pp.92-104.
[8] M. Oku, S. Nakamura, N. Hiramatsu and Y. Uematsu: Nisshin Steel Tech. Rep., 74, 1996, pp.26-36.
[9] M. Oku, Y. Fujimura, S. Nakamura, K. Itou, T. Nagoya and Y. Uematsu: Nisshin Steel Tech. Rep., 80, 2000, pp.32-39.
[10] A. Miyazaki, J. Hirasawa and O Furukimi: Kawasaki Steel Giho, 34, 2002, pp.81-84.
[11] H J. B. Alves, J A N. Carvalhop M V. Aquino and M J. Mantel: Proc. 4th European Stainless Steel Science and Market Congress Vol.1, ATS, Paris, 2002, pp.26-29.
[12] F. Chassagne, L. Antoni, O. Cleizergues, G. Lovato, M. Gardon and J L. Moiron: Proc. 4th European Stainless Steel Science and Market Congress Vol.1, ATS, Paris, 2002, pp.36-39.
[13] Y. Watanabe, K. Shiratani, M. Suzuki, S. Iwanaga and K. Nishino: TOYOTA Tech. Rev. 47, 1997, pp.108-113.
[14] P. O. Santacreu, H. Sassoulas, F. Moser, O. Cleizergues and G. Lovato: Thermal Stress ’99, 1999, pp.245-248.
[15] B. L. Choi, H. Chang and K. H. Park: Int. Journal of Automotive Technology, 5, 2004, pp.297-302.
[16] M. Oku, S. Nakamura, N. Hiramatsu and Y. Uematsu: Nisshin Steel Tech. Rep., 66, 1992, pp.37-48.
[16] S. S. Manson: NACA Tech. Note 2933, 1953, pp1-100.
[17] L. F. Coffin: Trans. ASME, 76, 1954, pp.931-950.

CORROSION SIMULATION TESTS ON STAINLESS FOR AUTOMOTIVE APPLICATIONS

B. Michel[1], S. Saedlou[1], J.M. Herbelin[2], P.O. Santacreu[1]

[1]ArcelorMittal Global R&D, [2]ArcelorMittal Stainless Europe, France

Abstract

Stainless steel is largely used in the automotive market, essentially for exhaust system. In that field of application, designs are more and more complex and the guarantee durations continuously increase. Thus laboratory tests were developed in order to simulate automotive environments and estimate their impact on stainless steel durability. Corrosion mechanisms greatly depend on the temperature and so the exhaust system could be divided in two parts which are: the hot part near the manifold (400<T(°C)<900) and the cold part near the muffler (20<T(°C)<400). For the hot part, the main corrosion mechanism is oxidation, also called dry corrosion. Laboratory test used for that high temperature application is the cyclic oxidation. The behaviour of each grade is evaluated through mass variation measurement on specimens exposed to a specific thermal cycle during x-hours. In the cold part, near the muffler, exhaust gas could condensate on the internal surface of the exhaust system to form complex acids. Consequently corrosion mechanism is more complex and is a combination of wet and dry corrosion. On that idea, a “dip & dry” apparatus was developed in order to simulate that kind of corrosion on stainless steel grades, by cyclic dipping in an artificial condensate, drying and oxidized specimens in oven. After test, grades are compared through maximum corrosion depth measures. In addition, the external cold part of the exhaust system is visible and so, guarantee could also include cosmetic requirements. An experiment test based on climatic standard test with periodic heat treatment at 300°C was developed to mimic the external corrosion of exhaust system. Thus treated specimens are evaluated thanks to a cosmetic observation based on comparison with reference samples. All these corrosion simulation tests permit to develop a complete ferritic stainless steel offer dedicated to the exhaust market.

Corrosion in the hot part of the exhaust system

Dry hot corrosion

Context

Closed to the manifold, thermal cycles and high temperature lead to very severe dry corrosion mechanism what could be detrimental for exhaust durability. In cyclic oxidation, not only classical chemical aspect of oxidation needs to be studied. Of course, a mechanical aspect has also to be taken into account because of thermal expansion difference between the metal and the oxide layer formed at high temperature. At high temperature, an oxide scale is formed on the steel surface, with a thickness following a parabolic law vs time. However, during cooling of the system, stresses are generated at the metal/oxide interface what could lead to oxide spallation. As this mechanism is repeated at every thermal cycle, it could cause important metal consumption [1-2].

Experiments

The principle of the test, described on Figure 1, permits to realize thermal cycles in accelerated conditions (Figure 2). The maximum test temperature depends on exhaust gas temperature measured on customer bench but with the improvement of engine performance, this temperature continuously increases up to 1000°C in extreme cases. Consequently the tests are carried out up to this temperature.

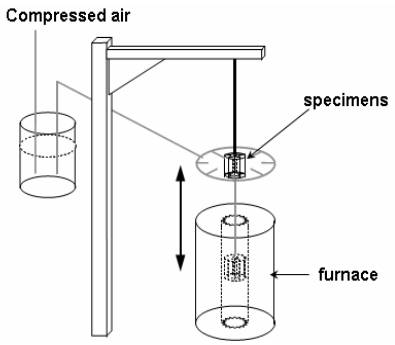

Figure 1. Schematic view of the cyclic oxidation test

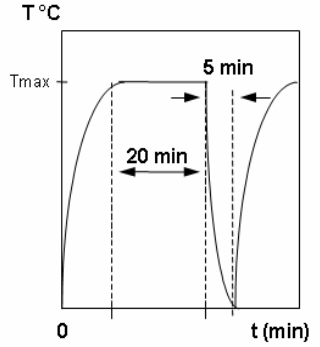

Figure 2. Thermal cycle used for exhaust application

Then samples are characterized by weight variation measurement versus time. The major observation highlighted on these results is the better behaviour of ferritic grades compared to austenitic (Figure 3). This is mainly due to the high thermal expansion of the austenitic compared to the ferritic one, what leads to higher stress concentration at the metal/oxide interface during cooling and then, higher oxide spallation rate.

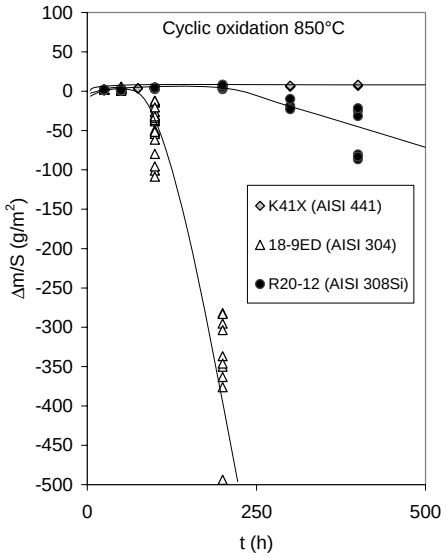

Figure 3. Weight loss measurement vs time on several grades with Tmax=850°C

DeNOx system effect : urea injection

Context

Due to the necessity to reduce NOx emission established by Euro 5 standard (2009), new equipments were developed for diesel vehicles (truck as well as car). The most promising

technology is called Selective Catalytic Reduction (SCR) and takes advantage of the reduction feature of ammonia (NH_3) on NOx.
As NH_3 couldn't be used for safety reasons (toxicity, flammability of ammonia) because the reactions take place inside the exhaust system, urea solution was selected to initiate the reaction. This molecule, by its decomposition at high temperature releases NH_3 species [3], what permits reduction of Nox as described on the following scheme:

$$(NH_2)_2CO \xrightarrow{heat} NH_3$$
$$+$$
$$NOx \xrightarrow{catalyst} N_2$$

Scheme of the catalyst reduction of NOx in SCR system from urea solution to nitrogen

Thus, urea solution is injected in the exhaust system by means of a spraying nozzle. As a result, some urea can enter in contact with internal shell of exhaust system at high temperature and then could cause damages on stainless steel.

Experiments

To get a better understanding of involved mechanisms and afterward to improve material selection, a laboratory test was developed at Isbergues Research center. The simulated test consists in spraying urea solution on cyclic heated stainless steel. After test, cross section analysis were performed on the specimens in order to determine the kind of attack observed and the metal depth which is affected. Depending on temperature and time conditions, we evidenced a carbonitriding mechanism as shown on the 304 grade thanks to cross section analysis with SEM (Figures 4, 5 and 6). That means urea decomposition on the surface of stainless steel at high temperature could leads to diffusion of interstitial species such as C and N in the metal.

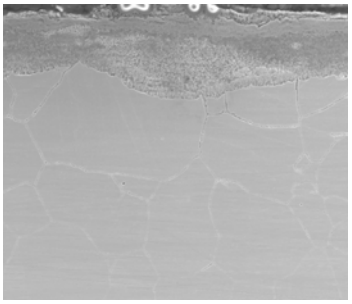

Figure 4. SEM observation of a 304 grade after 150h test 600°C

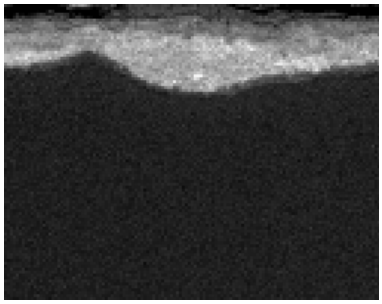

Figure 5. X Cartography of nitrogen

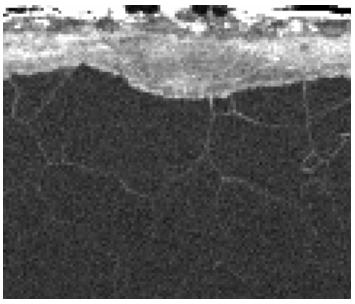

Figure 6. X Cartography of carbon

Corrosion in the cold part of the exhaust system

Internal corrosion

Context

In the cold part of the exhaust system, combustion gases such as SOx, NOx… combined with air humidity provoke condensation of an aqueous acid solution on the internal side of the shell (mix of sulfuric acid, nitric acid…). Consequently, this condensate could cause severe corrosion damages, mostly in the muffler where the evacuation of this acid solution is not facilitated. In particular, the most critical zones are the confined areas between shell and baffles, where crevice corrosion could develop and in extreme case, lead to perforation of the muffler.

Experiments

The test used at Isbergues Research Center to simulate the “internal corrosion” mechanism of the exhaust system is the so called dip dry test which has been especially developped for that application. It permits to simulate exhaust system environment by successive operations described as follows:

- Cyclic immersions and emersions into properly selected solution to simulate exposure to condensate (inner parts) in order to reproduce wet corrosion mechanisms.
- Step in oven simulating high velocity runs and reproducing high-temperature corrosion and oxidation mechanisms.

Different kind of cycles could be performed in order to simulate an urban or a highway type running. However, urban type cycles are the most agressive due to an important number of dip/dry steps compared to highway type cycles. In these conditions and in order to simulate the most critical areas of the muffler, an artificial crevice is fixed on the lower part of the specimen. After test, the artificial crevice is removed and the maximum corrosion depth in the confined area is measured. On Figure 7 below are presented the results obtained on stainless steel grades usually used for exhaust applications. These results allow to compare grades and thus to improve grade selection, depending on guarantee requirements.

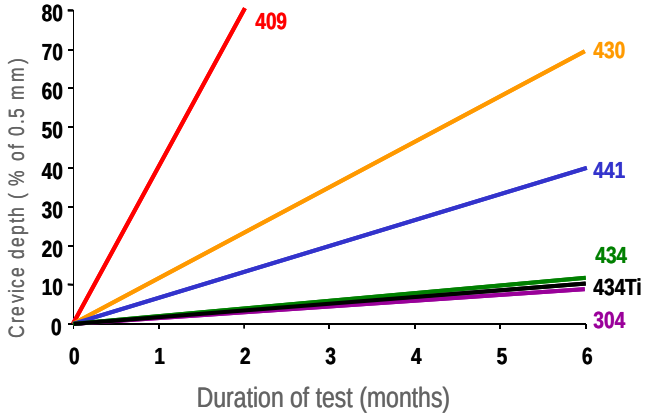

Figure 7. Maximum corrosion depth under artificial crevice after Urban cycle type on dip dry test at 300°C synthetic condensate pH4

Cosmetic corrosion

Context

Depending on the customer, some cosmetic demands could be requested for visible parts of the exhaust system. Effect of deiceing road salts combined with oxidation coming from gases temperature cause pitting corrosion of external parts of the exhaust system. Thus, products generated by these corrosion mechamisms could affect the general aspect through coloration of the steel and red rust appearance.

Experiments

This specific corrosion mechanism so called “cosmetic corrosion” is simulated through a cyclic corrosion in climatic chamber. The cycle is based on a classical automotive climatic test which simulates the external environment and use of a car (Figure 8). After test, samples are visually evaluated by means of a reference chart which evaluates visual deterioration due to both oxidation (coloration) and pitting corrosion.

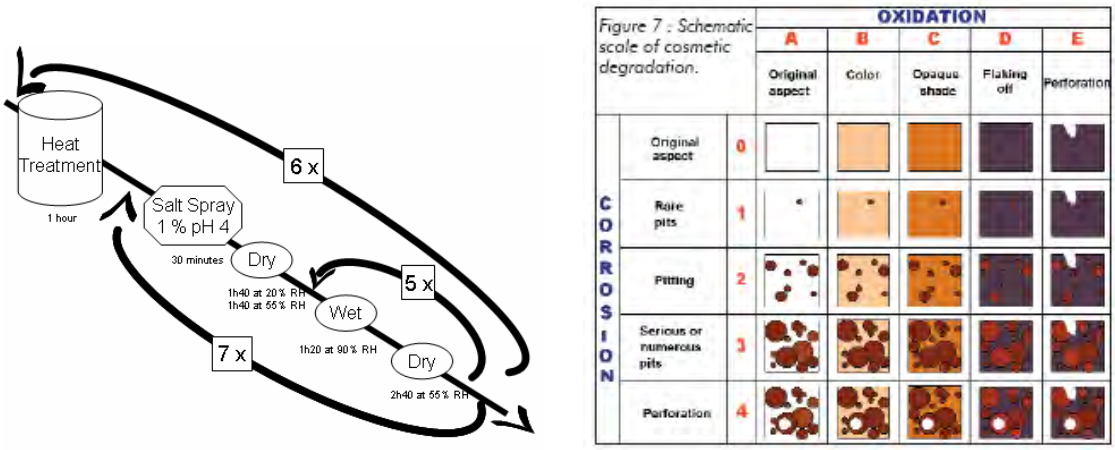

Figure 8. Cosmetic corrosion test and reference chart principe [4].

Based on their field of experience and their cosmetic requirements, customers are thus able to selected appropriated grades for their applications.

Concluding remarks

All procedures presented do not intent to establish an absolute ranking of stainless steel grade performance but they turn out to be efficient methods to characterize more precisely corrosion and oxidation damages undergone by exhaust system materials.
Besides, more exhaust line continues to evolve technically, in particular with the arrival of particulate filter for diesel, the down-sizing in engine and SCR depollution system, more new ferritic solutions are prefered.
Thus ArcelorMittal Stainless approach led to the definition of a complete ferritic offer specially dedicated for both hot and cold parts of the exhaust line able to fit in the same time the durability requirements and the increasing demand of guarantee.

References

[1] Antoni, L., Herbelin, J.-M., (1999), in EFC Working Party Report on Cyclic Oxydation of High temperature Materials : Mechanisms, Testing Methods, Characterisation and Lifetime Estimation M.Schütze, W.J. Quadakkers Eds, Publication N°27 in European Federation of Corrosion Series, Institute of Materials p.187

[2] Cyclic oxidation behaviour of stainless steels – appliation to the automotive exhaust lines, L.Antoni and B.Baroux, La Revue de métallurgie-CIT Février 2002, pp.178-188

[3] F. Birkhold et al. “Analysis of the injection of urea-water-solution for automotive SCR DeNOx-systems: Modeling of Two-Phase Flow and Spray/Wall-Interation”, SAE Technical Paper Series 2006-01-0643, April 2006.

[4] D.Guillou et al. “Cosmetic analysis of an exhaust system”, Ingénieurs de l’automobile, Juin-Juillet, 2002.

INNOVATIVE STAINLESS STEEL SANDWICH PANEL APPLICATIONS FOR TRANSPORT INDUSTRIES

M. Sirén[1], A. Gales[2], D. van Hoecke[3], R. Sánchez[4], J. Säynäjäkangas[5]

[1]VTT, Finland, [2]TNO Science and Industry, The Netherlands, [3]Ocas N.V., Belgium, [4]Acerinox S.A., Spain, [5]Tornio Research Centre, Outokumpu Tornio Works, Finland

Abstract

All-metal sandwich panels of three different basic configurations were manufactured of austenitic stainless steels by laser welding. The panels were subjected to exhaustive mechanical testing programme including constant load and four-point bending tests for full size 2.5 m^2 panels, and fatigue and crash testing of smaller panel sections. Reference panels were manufactured by adhesive bonding and by using insulating foam in a basic welded panel. All the panel types fulfilled the set requirements for the static, i.e. design loading, and fatigue situations – no requirements were preset for crash properties. Once the panel surface sheet thickness and total panel thickness are fixed, there are no significant differences between panel types, material strength or manufacturing routes from the load bearing point of view. The reason is that the practical structural properties are stiffness dependent. The differences in panel type, material strength or assembly method only become evident at loads and displacements way beyond acceptable in transport equipment service – apart from exceptional impact load situations, such as crash or collision. The choice between panel types has to be based on other issues, such as weight optimisation, ease and cost of manufacture, or aesthetics.

Introduction

The main advantage of using all-metal sandwich panels is the improved strength or stiffness-to-weight ratio as compared to solid sheet structures. This results from the increase of "apparent" thickness of the structure, i.e. bringing the outer surfaces further away from each other, which can be utilised as improved stiffness and load-bearing capacity. In an optimised panel, the core elements transfer the loads effectively between the skins while increasing the panel weight as little as possible. There is potential to drop the panel weight to a fraction of that of a solid sheet.

Some disadvantages exist with all-metal sandwich panels. Firstly, the manufacture of large panels with closed cross-section requires a keyhole technique, typically laser welding, which is capital intensive. This promotes series production of standardised panels, which decreases tailoring possibilities in smaller volumes – or favours the use of specialised sub-contractors. Secondly, the tube or sheet profile panel cores result into heterogeneity of stiffness and strength properties between panel plane directions that has to be dealt with in design. Thirdly, the feedthroughs or openings often lead into breaking of core elements, which affects the panel properties. Thus, the ideal areas for all-metal sandwich panels are weight critical load carrying applications that include large total areas of similar panels with few or no feedthroughs required. Train and metro car floor structures are examples of such applications. The work described here was carried out in a European project "Development of lightweight train and metro cars by using ultra high strength stainless steels (DOLTRAC)", ECSC contract 7210-PR-363.

Materials

The starting point for the panel design and dimensioning were the recent stainless steel material developments, and the design data given by the project industrial support group from an existing metro car. The materials were austenitic stainless steels EN 1.4318 (AISI 301 LN) in C850 and C1000 conditions and "304 SP" in 2B condition. Typical of the former is the high strengthening rate as a result of moderate cold rolling reductions, and the latter one is a new version of the 304 type with enhanced pitting resistance by reduced Mn and S, and increased Mo and N contents.

Design

The given static design loading case was 480 kg/m^2 constant load plus a 1.5 kN local point load, resulting in less than L/300 deflection. Another loading case was defined for fatigue, but no preset criteria existed for crash behaviour. The aim was to maximise the load bearing capability and minimise the weight of a sandwich panel made of 1.25 m wide strip by optimising between panel types, material strengths and panel lengths, four each. The dimensioning programme used for initial screening calculates a weight optimised sandwich structure for set loading conditions. The panel is idealised as a beam between webs with the core parallel to beam length. The panel and sheet thickness as well as distance between core elements were varied in small increments. The four basic sandwich types included in these calculations are in Figure 1.

Figure 1. Schematics of the panel types evaluated in the design phase.

The calculations were made in two phases: first, a relatively large material, thickness and panel dimension variety was screened to find the lightest alternatives. Based on the results another round focused on material combinations and geometries most favourable from the material production and manufacturing point of view. As a result, three panel designs with material details were defined. Unfortunately, switching from theoretically optimised designs to industrially viable ones results in considerable punishment in both panel weight and displacement under loading, as can be clearly seen in Figure 2.

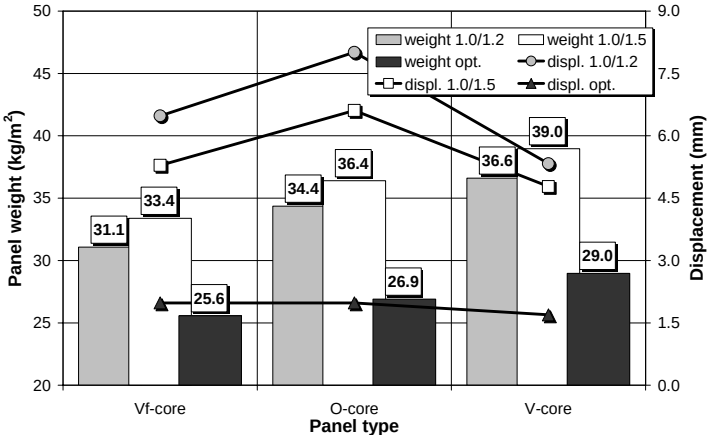

	Panel type		
	O	V_f	V
Top sheet (mm)			
1.4318 C1000	1.9	1.9	1.9
Core (mm)			
geometry	20×50	60°	60°
304 SP	1.0	1.0	1.0
1.4318 C850	1.0	1.0	-
Bottom sheet (mm)			
1.4318 C1000	1.2	1.2	1.2
1.4318 C850	1.5	1.5	-

Figure 2. Panel weight and displacement comparison between optimised and selected experimental panels. The legend figures, indicate the core / bottom sheet thicknesses in mm. Web spacing is 2.0 m and the point load area 10 × 10 mm^2. Each panel type was manufactured in all combinations of the details in the table on the right.

As for the panel weight, the increase is about 25% with a 1.2 mm bottom sheet, and about 33% with a 1.5 mm one. The differences are even greater when considering the displacements that are doubled or even tripled in most cases. Since the optimisation is based on elastic deformations, the use of harder bottom sheet materials will not bring any changes to the situation. As a result of this design phase, the final panel dimensions were fixed to ~ 53 mm × 1250 mm × 2200 mm and other details as described in Figure 2.

Panel manufacture

Expertise and experience in all-metal sandwich panel manufacture has been created in a recent Finnish national technology programme on lightweight structures. This was utilised to realise nine series of different panel type - material combinations with five panels each. Variations to these 45 1.25 × 2.2 m^2 panels were brought introduced by adhesive bonding in one V_f panel and filling another with insulating foam for reference.

The RHS tube core elements of the O panels were manufactured in a commercial production line into custom dimensions required. The V_f and V cores were manufactured manually in automatic edging presses. Especially for the latter ones this route showed extreme difficulties. Even the smallest inaccuracies cumulated towards the edge of the wide core element, thus making the tolerance control and panel assembly by laser welding very difficult. For V_f panels this was not a problem, because the tight tolerances were easily achieved for relatively narrow individual core elements. For both of these panel core types roll-forming would be a more manufacturing feasible method provided the production series are large enough.

To avoid the visible weld or tint mark on the weld root side that may be aesthetically unacceptable, one V_f type reference panel was manufactured by adhesive bonding with two component epoxy. In practical applications sandwich panels have functions other than just carrying load, too. One is to insulate the vehicle interior from ambient temperature and noise. Since the insulation characteristics of a pure metallic structure against these factors are poor, one laser welded panel was filled with a two component polyurethane foam for comparison with an empty panel. Panel filling is expected to bring some extra stiffness as well.

Panel testing

The panels were designed to minimise their weight for a predetermined loading conditions, 480 kg/m^2 constant load combined to 1.5 kN point load with deflection displacement of L/300, i.e. 6.67 mm for 2000 mm span length. Apart from design load verification of full-size 1250 mm × 2200 mm panels, the ultimate strength was measured in four-point bending. Smaller, approximately 500 mm × 1000 mm panel samples were tested in three-point bending under static and fatigue loading, and (200 – 400) mm × 1800 mm sections in quasi-static and crash tests. The fatigue testing case was based on the static load of a 2.5 ton train car underfloor equipment box mounted with eight brackets, superposed by ± 20% dynamic loads. Thus, the specified fatigue load was 3 000 N ± 600 N (R = 0.67) subjected on an area of 100 × 100 mm^2 for 10^7 cycles.

Desing load testing

The loading situation combining both constant and point loading required a special test arrangement. This system called the “vacuum box” utilises the pressure difference between ambient pressure and vacuum underbeath the panel. From the results it can be concluded that all the tested O- and Vf-panels easily fulfilled the design load criteria: to reach the L/300 displacement required 3 to 4 times the design load. The adhesively bonded demonstrator panel performed excellently as compared to the laser welded ones: the displacements were the smallest of V_f-panels and at the same level with the best O-panels, which are heavier constructions.

Four-point bending tests

Altogether 18 full-size O- and V_f-type panels were tested in four-point bending. An effort was made to evaluate of the panel elastic behaviour by determining the slope of the load-displacement curve of each panel at the elastic region. Both the panel types show – within reasonable scatter – a same range of slope that depends above all on the bottom sheet thickness. An increase from 1.2 to 1.5 mm results in a 15 to 20% higher slope value. In the optimisation calculations the decrease in displacement caused by the change of bottom sheet thickness from 1.0 mm to 1.5 mm is about 18%, i.e. comparable to the experimental results. A representative load-displacement curve for each panel type and variant can be seen in Figure 3a. Noteworthy is that the elastic behaviour is practically the same for both panels with 1.2 mm bottom sheet, whereas the difference is greater for 1.5 mm sheet panels. A performance comparison between various laser welded and adhesively bonded panels in Figure 3b.

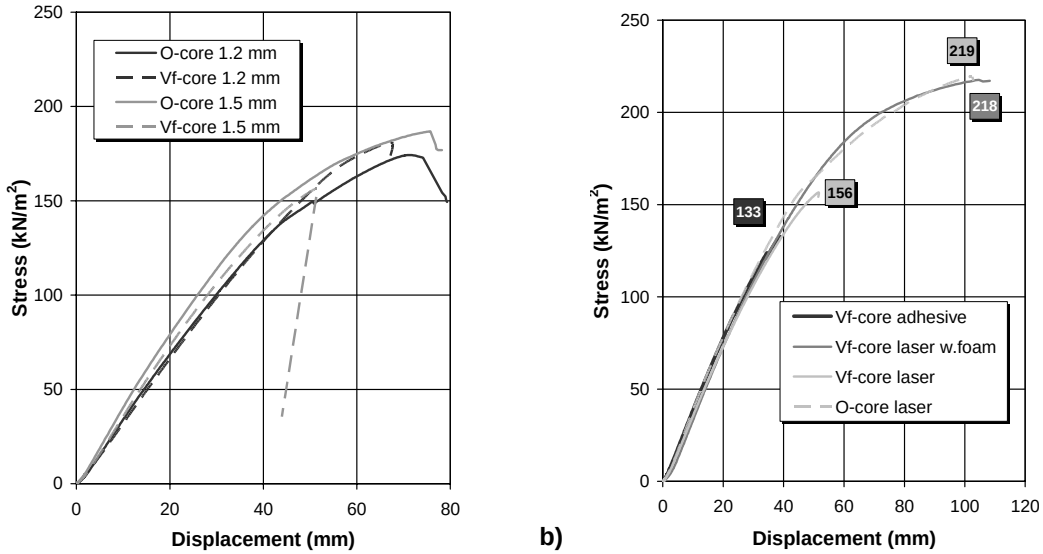

Figure 3. a) Typical load-displacement curves of various panel types showing the effect of bottom sheet thickness on stiffness; b) The load-displacement curves and maximum loads of different types of panels with 1.5 mm 1.4318 C850 bottom sheet and continuous laser welds as compared to ahdhesively bonded reference.

As a conclusion it can be said that once the panel surface sheet thickness are the same, there are no significant differences in the applicability between panel types or manufacturing routes from the load bearing point of view. The differences become evident at loads and resulting displacements that are way beyond acceptable for any floor structure. However, the improved maximum load bearing capacity may be utilised in exceptional impact load situations, such as crash or collision. Thus, the choice between panel types has to be based on other issues, such as the advantages of using standard RHS tube cores instead of tailored sheet V_f profiles against the punishment in panel weight, or the smooth and intact sheet surfaces available by using adhesive bonding against the increased panel assembly time and uncertainty of the long term durability of adhesive joints.

Three-point bending tests

The three-point bending test was originally designed for fatigue testing of panel sections: it was foreseen that performing fatigue tests for full-size panels would bee too resource intensive. A limited number of static bending tests until fracture were done to compare all the three panel types in bending and to gain data for fatigue test arrangements. Apart from longitudinal ones, transverse sections were to be tested, but because of excessive displacements leading into very low frequencies and long test durations, they were dropped off. The panel section dimensions

were a compromise between load frame column spacing and odd number of core elements to introduce the loading tool on a core instead of free sheet surface. The result was 500 mm section width and 800 mm span length accommodating five longitudinal tube and three V_f elements.

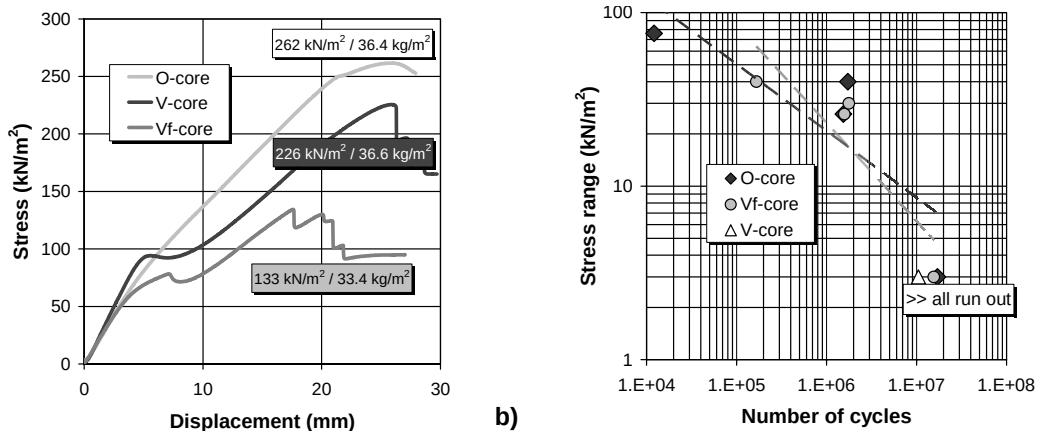

Figure 4. a) Load-displacement curves and panel weights of three panel types; b) Panel section fatigue results.

From the longitudinal three-point bending test results in Figure 4a it can be clearly seen that the V-core panel is the stiffest one at the elastic region, which is the most important area regarding the practical load-bearing applications. The force required to achieve an L/300, i.e. 2.67 mm displacement is about 50% higher than for the O- or V_f-type, and the slope is about 20% steeper, even if the bottom sheet is thinner 1.2 mm one.

As mentioned earlier, the defined fatigue loading situation was 10^7 cycles fatigue life under a 7.5 kN/m^2 ± 1.5 kN/m^2 load (R = 0.67). As can be seen in the fatigue results of Figure 4b, all the panel types survived the fatigue loading criteria. For V-type panels, this verification was also the only one performed. Results at higher loads for O- and V_f-panel show that a fatigue life of 10^6 cycles is realistic for them in practise under 63 ± 13 kN/m^2 loading. Above this level, the initial core buckling confuses the situation, but at least the O-core panels show potential for even higher loads. Despite of the promising results, care should be taken in drawing any further conclusions of the panel fatigue properties because of the extremely limited number of specimens tested.

Panel compression and crash testing

Quasi-static compression tests were carried out for panel sections to determine the buckling strength and buckling mode for background information for dynamic crash of the panels. Panel deformation consists of two parts in this case: below the buckling load very large forces but small axial displacements result in small elastic energy absorbing capacity; only the modulus of elasticity, moment of inertia of the cross-section and panel length are relevant parameters. After the buckling load (post-buckling), the panel will develop plastic deformation and energy is absorbed in the panel; yield strength, hardening behaviour, strain rate sensitivity, ductility and buckling modes are the relevant parameters.

The static tests were limited to O-core and V_f-core only because there was only a limited amount valid V-core panels available for both static and dynamic tests. The test tests were performed like described in a pseudo simply supported way and under quasi-static testing conditions. From the start of the test the welds were clearly audibly cracking with both O- and V_f-core panels, and maximum normalised energies of 2.5 and 1.9 J/mm, respectively, were measured before buckling, Figure 5a. Theoretically, the diference should have been about one third of this for

O-panels, and the maximum loads should have been double the measured for both types. In the transverse tests the maximum force is only a fraction of the longitudinal tests, Figure 5a, and the V_f-panel shows about double normalised buckling energy to O, as expected.

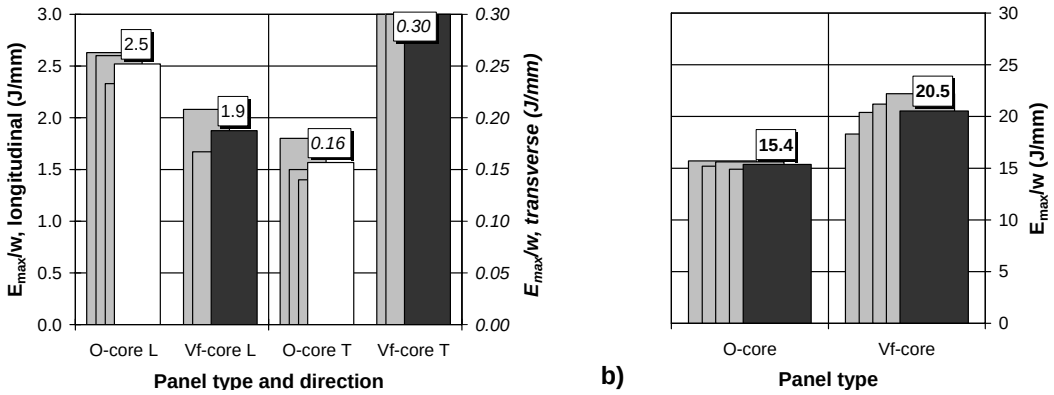

Figure 5. a) Quasi-static panel compression test results L = longitudinal and T = transverse; b) Panel transverse crash test results. Normalised energies are used because of varying panel section widths.

For the crash tests a rig was used with a 267 kg ram launched by means of pneumatic cylinder up to maximum of 9.5 m/s, corresponding to 11 kJ kinetic energy in the ram. The ram is slid along the rails on sliding pads, and the speed is measured just before impact. The panel is clamped in a pseudo simple supported way. Because all panels absorbed the full amount of energy given to them in the longitudinel tests, only minimum performance values can be given: at least 55, 40 and 60 J/mm of energy can be dissipated by O, V_f and V panels of this type, respectively.

In the results for the transverse tests in Figure 5b, there is a significant difference between O and V_f-core panels tested at the same speed. This is well in line with quasi-static tests and can be explained by the contribution of the cores in the energy absorption: V_f cores allow more elastic deformation and thus convert kinetic energy more effectively to elastic deformatio – indicated by ram bouncing – whereas O-cores guide the energy into plastic deformation in surface sheets.

A significant difference between buckling modes was detected: in the static test the global buckling mode was mainly activated while in the crash test local buckling was predominantly present at the panel ends.

Summary and conclusions

It can be concluded that all the panel types fulfill easily the set requirements for the static design and fatigue loading situations. However, the panel optimisation calculations gave excessive displacement values as compared to the experimental ones. In other words, there still remains potential for further weight saving in these panels.

Once the O- or V_f-panel surface sheet thickness and total panel thickness are fixed, there are no significant differences between panel types, material strength or manufacturing routes from the load bearing point of view. The practical structural properties are stiffness, i.e. geometry dependent and the differences in panel type, material strength or assembly method only become evident at loads and displacements far beyond acceptable for any floor structure. Thus, the choice between panel types and details has to be based on other issues, such as weight optimisation, ease and cost of manufacture, or aesthetics.

In static longitudinal compression tests global buckling is the major failure mode while in the crash tests local buckling at the panel end governs leaving the middle of the panel almost without

any deformation. The lack of lateral deformation leaves intermediate areas unharmed, which is the most favourable condition for the passenger space in terms of crash worthiness. In transverse tests the panels showed more widespread plastic deformation in both static and crash tests, clearly visible by large lateral deformation that also reduce the passenger space considerably.

Acknowledgement

The financial support of the EC is acknowledged in the project “Development of lightweight train and metro cars by using ultra high strength stainless steels (DOLTRAC)”, performed under the ECSC contract 7210-PR-363.

STAINLESS STEEL REBAR: A DURABLE AND COMPETITIVE SOLUTION AGAINST CORROSION

B. Demelin[1], F. Moulinier[2]

[1]Ugitech, France, [2]Institut de Développement de l'Inox (I.D.Inox), France

Abstract

The main reason of the defacement of the constructions is the corrosion of the reinforcement bars, which is mainly due to the carbonation of the concrete and/or to the penetration of chlorides through the concrete.The volume of the rust being about 6 times bigger than that of the steel, it exerts a pressure and the concrete bursts. Therefore it is an absolute necessity to prevent corrosion; the most frequently used solutions against corrosion are:

- To increase the concrete cover up to thicknesses of 50 to 60 mm
- To use sacrificial zinc anodes
- To paint the constructions with corrosion inhibitors
- Periodic chlorides extraction
- Cathodic protection

Use of stainless steel rebars is also a solution but insufficiently used, probably because it is perceived as being expensive and because of a poor knowledge of this material. However, it has many advantages compared with the other solutions such as:

- a much better durability
- requires lower amounts of materials
- safer
- environmentally friendly
- and finally very competitive regarding the whole life cycle

Up to now, a lot has been done for a better knowledge and for the promotion of stainless steel rebar:

- there exist national standards in most of the countries and a EN standard is in progress
- many research works on corrosion behaviour of stainless steels when embedded in concrete have been achieved
- studies and research on bonding properties
- studies and simulations on mechanical characteristics in case of seisms for instance
- and a lot of brochures and communications in conferences.

The results are encouraging regarding in particular some emblematic realisations. But if we consider the potential market which, according to the concrete specialists, is 1% to 3% of the total volume of the carbon steel rebar, this is to say between 1 and 3 millions tons, we are very far from this target.

There is still plenty to do and in particular:

- improve our knowledge on fatigue resistance
- run tests on fire resistance which we know is much higher than that of carbon steels
- give solid data on seismic resistance and shock resistance
- give solid data on the comparison of global cost

These results would significantly strengthen our positions in front of the decision makers by giving a response to the questions we are asked, by pointing out more news advantages of stainless steels, and give us more arguments to largely communicate.

Introduction

According to the civil engineering works or building experts, the main cause of the defacements of the constructions is the corrosion of the reinforcement bars embedded in the concrete. These damages have serious consequences in particular on the safety of the works, on the costs of maintenance, on their durability. This is why the corrosion of the reinforcement bars has become a major topic in the last few years, as shown presentations in the literature or in the conferences (fib congresses, consec' –concrete under severe conditions- conferences, dbmc –durability of buildings mateirals of conconstruction, etc.). At the same time the emergence of some new concepts such as sustainable development or global cost, make constructors and designers more aware of the necessity to avoid corrosion of the rebars. In addition to that, in Europe, the Eurocodes - new construction standards- principally based on the durability of the constructions, are now applied. For all these reasons corrosion of the rebar is not anymore a fatality and solutions have to be operated.

There already exist many solutions in order to avoid corrosion of the rebars: use of sacrificial anodes, use of corrosion inhibitors, chloride extraction, cathodic protection, increase of the concrete cover, galvanised reinforcement bars. Experience shows that none of these solutions is totally satisfactory, for the most efficient ones are very expensive and the cheapest ones are most often very inefficient.

If we compare the stainless steel rebar experiences with the other solutions, it appears that they present many advantages: higher durability, no maintenance requested, better global cost, etc. Hence, finally stainless steel rebar is a very valuable solution which in most cases should be preferred and stainless steel rebar should be very widely used.

The experts of the concrete industry (French CERIB) consider that the amount of reinforcement bars affected by corrosion (worldwide) represents between 1% and 3% of the total, i.e. between 1 and 3 million tons per year, which represents the potential market for stainless steel rebar. However, we must admit that with exception of some emblematic recent construction sites, the use of stainless steel rebar is still very insufficient.

Tiny market share facing the other solutions for a superior product: Why and what to do?

Corrosion of the reinforcement bars

There are in general two main causes for the corrosion of the carbon steel reinforcement bars: carbonation and chloride penetration; aggressive chemical products also generate corrosion in waste water treatment plants or industrial zones.

Carbonation

The pH of fresh concrete is generally around 13 due to a high concentration of alcaline products of KOH, NaOH and $Ca(OH)_2$; in these conditions the carbon steel reinforcement bars are passive; but in wet environments, due to the combined effect of the CO_2 adsorption and the water, there is a chemical reaction leading to the formation of $CaCO_3$ and diminution of $(OH)^-$ ions concentration:

$$Ca\,(OH)_2 + CO_2 + H_2\,0 \rightarrow Ca\,CO_3 + 2H_2O$$

Consequently, the pH decreases, and when it reaches the value of about 10, carbon steel bars loose their passivity and corrosion starts. The volume of the rust is about 6 times larger than that of the steel, so that it exerts a strong pressure and the concrete, which doesn't resist tensile forces, may burst. At the same time the bars lose their mechanical resistance and the entire construction becomes less resistant.

Chloride penetration

In marine environments or on the works exposed to deicing salts, there is a high chloride concentration. These ions, very small, penetrate through the concrete, which is always more or less porous, and when they reach the carbon steel reinforcement bars, corrosion starts.

The solutions to avoid corrosion

There exist many solutions in order to prevent or avoid corrosion of the carbon steel reinforcement bars. The most classical ones are:

To increase the concrete cover thickness and/or to use compacter concrete

This solution delays the chloride penetration rate and in case of carbonation it delays the decrease of the pH in the concrete, which is in contact with the bars. This solution is relatively efficient, but never totally prevents corrosion. This is recommended in the Eurocode 2 in Europe when stainless steel rebars are not used. Nevertheless, finally corrosion always reach the bars which corrode. This method has some other inconveniences: if the cover is too thick, there is a high risk of appearance of cracks, which facilitates the corrosion product penetration through the concrete. Other weakness of this solution: it consumes greater amounts of concrete and/or in the case of compact concrete the products are much more expensive. With greater amounts of concrete the infrastructures are heavier and consume more materials.

Corrosion inhibitors

This solution consists of putting a coat of a chemical product, which pentetrates through the concrete and protects the reinforcement bars against corrosion. In theory it is supposed to work, but in practice, experience shows that, after several years of tests, their effectiveness is not proven. New test methods on new products should be applied in the next few years, but experts are becoming more and more sceptic about this solution.

Chloride extraction

This solution based on predictive models on the chloride penetration rates protects the construction against the chlorides, provided that it is done periodically, but not against carbonation. It has to be repeated regularly and it must be done very thoroughly. Hence, it is rather expensive during the whole service life of the work. In practice, this solution is used for the most ancient constructions, which were built without any precaution against corrosion. On new buildings, designers prefer a durable preventive solution against all types of corrosion: chlorides and carbonation.

Sacrificial zinc anodes

Judiciously placed zinc anodes on the reinforcement carbon steel structure protect efficiently the reinforcement system. It is a cheap and easy solution provided that the number of anodes is sufficient and provided that they are placed in order to effectively protect the reinforcement bars; the advantage of this method is that it is relatively cheap and easy to work out at the erection of the construction. However, it has major inconvenients: the life time of the anodes is generally not beyond 12 to 15 years, which means that they have to be replaced very frequently; the replacement of the anodes is generally a costly maintenance operation (necessary to put the work

temporarily out of order, to break the concrete, to extract the consumed anodes, provided that there is a precise map of where they are placed...).

Cathodic protection

The principle consists in sending a permanent electric current opposite to the corrosion current in order to electrically protect the carbon steel rebars. This method, when correctly worked out, is very efficient and works very well; experience shows that in good conditions works are very well protected against all types of corrosion: carbonation, chlorides and chemical.
This process has to be installed by very skilled operators, because if not well done, the results may become very rapidly desastrous with an acceleration of the corrosion instead of a protection in some places; it also requires a permanent monitoring and, if for any reason the current stops, then corrosion starts. Actually, some specialised companies are highly qualified for this type of protection, and the life duration of this solution can be up to 40 to 50 years. But on the other hand, this method is in general the most expensive: necessary to have a very qualified (hence, expensive) supplier, high costs of installation, permanent monitoring.

Reinforcement bars protected against corrosion

Regarding the existing solutions to protect rebars, it is possible to mention:

- epoxy coated bars; they have been tested but they cannot work at least for two reasons: insufficient bonding characteristics and the coating may be damaged by a scratch, thus reducing seriously their corrosion resistance
- galvanised bars; they have the major inconvenience that in a pH of 12 or 13, i.e. in fresh concrete, the coating is not resistant to corrosion and the layer is attacked; and the cut ends of the bars are not protected against corrosion
- some experiments are made on fiberglass bars: they have obviously a very good corrosion resistance, but they cannot be bent nor welded and their mechanical resistance is not sufficient
- then, why not stainless steel rebars?

Stainless steel rebar

A solution proposing steel rebars which are simply corrosion resistant in all conditions seems very attractive. But constructors and designers in a first approach ask many questions, as follows.

Are they really corrosion resistant?

Experience and laboratory tests show that they are corrosion resistant in all conditions of use of concrete works:

- in carbonated concrete because the pH is ever over 8;
- in chloride environments, provided the grade is adapted
- in chemical environments such as water treatment plants
- even if a part of the concrete has been damaged and if the bars are directly in contact with the environment they resist to corrosion.

What are their bonding characteristics?

According to the standards, the bonding characteristics of the steel reinforcement bars depend on their surface geometry. Stainless steels belong to the family of steels and if the geometry of the ribs is in conformity with the standards, then the bonding characteristics are satisfactory; bonding characteristics of stainless steel rebars have been tested in laboratories: “pull in” and “pull out” tests are satifactory.

Can they be worked out like carbon steel rebars?

The conditions of use are very similar to those of carbon steel rebars; some differences must be taken into account and some precautions must be taken such as:

- higher mechanical resistance, which means that they are more difficult to bend
- a spring back when bent
- welding parameters have to be modified
- contamination by iron particles should be avoided.

What are their mechanical characteristics?

Stainless steel rebars have higher mechanical properties than carbon steel rebars have:

- yield strength currently over 500 MPa and up to 800 MPa for duplex, while for current carbon steels the maximum yield strength is 500 MPa
- high elongation especially for austenitic grades
- high energy absorption capacity taht is a significant advantage for seismic applications.

Are stainless steel rebars standardised?

Stainless steel rebars are standardised in most European countries and in USA. An European standard (EN) is in processing stage and may be published by 2009. In the European standard draft there are links with Eurocode 2 and with EN 206 in particular it allows to choose the proper grade according to the exposure conditions.

Can they be used partially, and in this case, is there no risk of galvanic corrosion?

Most of the time it is not necessary to use 100% of stainless steel rebar in the constructions; it is recommended to use stainless steel rebar partially on the most exposed parts and close to the surface. In this case stainless steel rebars are mixed with carbon steels and a risk of galvanic corrosion may occur. The studies on this question show that the potential difference between carbon steel and stainless steel is rather low and that if the number of contact points between the two materials is sufficient, then the risk of galvanic corrosion is globally low. At the same time it has been observed that the corrosion current between corroded carbon steel and stainless steel is lower than that between corroded carbon steel and stainless steel. Hence, provided some simple precautions are taken, it is possible to mix stainless steel rebar with carbon steel with a minimum risk of galvanic corrosion.

Are stainless steel rebars economically competitive?

If we consider just the difference of purchasing price between stainless steel and carbon steel, then stainless steels seem tremendously expensive, but this has no sense, because stainless steels are not used to replace carbon steels but as a solution in order to prevent corrosion; then the extra cost of stainless steels, partially used, in a construction has to be compared with the price of the other solutions against corrosion.

Most of the experts consider now that cathodic protection is the most efficient of the existing solutions, so we eliminate the other solutions which last in general between 12 to 20 years maximum; this solution requires important costs of monitoring, managed by a specialised company, its life duration is 50 years maximum, and it requires important costs of running; it is generally accepted that after about 20 to 30 years stainless steel rebar solution costs less than cathodic protection. After 40 to 50 years cathodic protection requires important investments for refurbishment but stainless steels doesn’t require any extra cost.

Considering the global cost stainless steel is probably the most competitive solution against corrosion, but this has to be proven by references.

Why are stainless steel rebars not more widely used? What to do?

Regarding their remarkable advantages compared with the other solutions, stainless stel rebar should be very widely used; yet there are not, and for some possible reasons:

- first they are perceived as expensive mainly because people just compare their purchasing price with that of carbon steels, which means nothing because they have to be compared with the other solutions against corrosion
- too many designers and constructors have not yet integrated the concept of global cost; the new Eurocode 2 clearly integrates this concept and there is a strong opportunity to catch for the promotion of stainless steel rebar; it is important to give the proof that the global cost of the stainless steel rebar solution is very competitive: this is why an WG group has been formed in order to give examples
- Stainless steel rebars are also perceived as rather complicated because there are many possible grades and the rules seem a bit difficult; the draft of the new european standard has taken this into account and simplifies a lot the grade selection and the conditions of use
- Some data are still uncomplete or missing about fatigue resistance or fire resistance; we all think that they are more favourable than for carbon steels but this has to be proven through studies and publications
- Users need examples of use with complete reports; there are now some examples the oldest one being the pier in Yucatan Mexico; the other examples are more recent but most of them built after the 1970; it should be useful to communicate inspection reports on a maximum of examples
- Most of the time it is clear that designers and constructors either ignore the the existence of this solution or have wrong ideas on its advantages compared with the other solutions especially in terms of cost. It is an absolute necessity to be better known by the contractors and designers by attending and speaking in the specialised conferences, by publishing articles as often as possible in the specialised magazines. Our competitors, in particular from the cathodic protection do it, why shouldn't we do the same? It is the best way to be better known and appreciated.

References

[1] Collection technique CIMBéton T.81 – I.D.Inox and CIMBéton- Béton armé d'inox: le choix de la durée

[2] CEFRACOR minutes of the "commission bâtiment du 7 février 2007"

[3] fib congress Naples June 2006: proceedings

[4] fib congress Dubrovnik May 2007: proceedings

[5] GC 2007 meeting Paris march 2007: proceedings

[6] Consec'07 conference Tours june 2007: proceedings

[7] French standard XP 35014

[8] M. Pedeferri, T Pastore, M. Gastaldi, and al. effects of chemical composition on corrosion behaviour of stainless steels in chloride contaminated and carbonated concrete, Proceedings stainless steel science and market, 3rd European congress, Cha Lagunia Sardinia, Italy

[9] S. Qian, D. Qu, G. Coates, Galvanic couipling between carbon steel and stainless steel reinforcements, National research council Canada –NRCC 48162- Aug 2005

[10] Dbmc (durability of buildings and mateials of construction) meeting Lyon, April 2005 proceedings.